

**Development of an Experimental Setup to Measure the Effectiveness of
Mechanical Filters For Nanoparticles**

Pooya Abdolghader

A Thesis
in
The Department
of
Building, Civil and Environmental Engineering

Presented in Partial Fulfillment of the Requirements
for the Degree of Master of Applied Science (Building Engineering) at

Concordia University
Montreal, Quebec, Canada

November 2018

CONCORDIA UNIVERSITY
School of Graduate Studies

This is to certify that the thesis prepared

By: **Poova Abdolghader**

Entitled: **Development of an Experimental Setup to Measure the Effectiveness of Mechanical Filters For Nanoparticles**

and submitted in partial fulfillment of the requirements for the degree of **Master of Applied Science (Building Engineering)**

complies with the regulations of the University and meets the accepted standards with respect to originality and quality.

Signed by the final examining committee:

Dr. S. Li Chair

Dr. I. Karimfazli Examiner

Dr. A. Soliman Examiner

Dr. F. Haghghat Thesis Supervisor(s)

Dr. A. Bahloul

Approved by Dr. F. Haghghat
Chair of Department or Graduate Program Director

Dr. A. Asif Dean,

Date November 28, 2018

ABSTRACT

Development of an Experimental Setup to Measure the Effectiveness of Mechanical Filters For Nanoparticles

Pooya Abdolghader

Nanoparticles (NPs) are particles of less than or equal to 100 nm in diameter. Due to their size, they have a significant effect on health and safety of people. Capture of these NPs in general ventilation systems by filters remains one of the most widely used means of protection due to its relative simplicity of implementation and its effectiveness for capturing various size of particles. In North America, filters used in general ventilation systems are tested by the ANSI/ASHRAE Standard 52.2 and are graded according to their efficiency, which is a function of particle diameter. However, the current standard limits the filtration efficiency assessment for particles between 0.3 and 10.0 microns. There is therefore a significant lack of knowledge about the behavior of these filters with respect to the particle diameter below 0.3 μm . The main objective of this study was to develop a measurement procedure to evaluate the effectiveness of mechanical filters used in general ventilation systems against (NPs). In this regard a small setup was designed, build and qualified. Then measurement procedure was validated by comparing the penetration measurements with those obtained on qualified big loop setup, which was inspired by ASHRAE setup for nano-metric particles. One type of mechanical filter rated (MERV 8) in three depth sizes (1, 2 and 4in) is used to illustrate the full penetration range that can be measured on both setups. The obtained results are consistent with the classical filtration theory for mechanical media and with previous experimental measurements on media and filters. The data presented in this study show that the particle range of 22.1-294.3 nm gives a fairly good correlation ($R^2=0.898$) between the two setups

and for the penetration range of 0.7-1.0 at two face velocities of: 1 and 0.75 m/s. The outcome results from this study is a firm validation to evaluate the effectiveness of mechanical filters used in general ventilation systems against nanoparticles.

ACKNOWLEDGMENTS

First and foremost, I would like to express my deep gratitude to my supervisor Dr. Fariborz Haghighat and my co-supervisor Dr. Ali Bahloul for all support, research guidance, inspiration and patience over the last two years of my study. I am and will always be sincerely grateful for the opportunity they gave me for realizing this project. The freedom that they gave me and they trust in my abilities were really rewarding for me.

I would like to thank other members of this research project; Dr. Clothilde Brochot, post-doctoral fellow at Concordia University. Her expertise, kindness, and confidence in my work were really appreciated. Much appreciation also goes to technicians Pierre Drouinas, Christian Sirard, Joseph Hrib and Luc Demers; for all their technical help to build and develop the setups.

Many thanks to the Institut de Recherche Robert-Sauvé en Santé et en Sécurité du Travail for supporting this project.

I am also very grateful to all my colleagues at the Concordia University sharing their knowledge and experience while providing me such a friendly environment, so remarkable and worthy.

Last but not least, I am deeply thankful to my father, Abdolsamad Abdolghader, my mother, Fatemeh Ghasabifard Zanjani, my brother, Pedram Abdolghader and my partner, Parisa Akbarimalkeshi for their continuous support and encouragement. This Master's degree would not have been possible without their love and support.

TABLE OF CONTENTS

ABSTRACT.....	iii
ACKNOWLEDGMENTS	v
TABLE OF CONTENTS.....	vi
LIST OF FIGURES	viii
LIST OF TABLES.....	ix
LIST OF ABBREVIATIONS.....	x
LIST OF SYMBOLS.....	xi
Chapter 1: INTRODUCTION.....	1
1.1. Background.....	1
1.2. Research Objective	1
1.3. Thesis Outline.....	2
Chapter 2: LITERATURE REVIEW.....	3
2.1. Introduction.....	3
2.2. Filtration capture mechanisms	4
2.2.1. Initial filtration efficiency of fibrous media.....	5
2.2.2. Filtration efficiency of clogged fibrous media.....	20
2.3. Pressure drop of flat fibrous media	21
2.3.1. Pressure drop of clean flat fibrous media.....	21
2.3.1. Pressure drop of clogged flat fibrous media	24
2.4. Estimating the packing density of the deposited particles (α_{pc})	31
2.5. Parameters affecting nanoparticle filtration efficiency	32
2.5.1. Effect of face velocity and air flow rate.....	32
2.5.2. Effect of humidity	33
2.5.3. Effect of particles shape and morphology.....	35
2.5.4. Effect of fiber diameter	37
2.5.5. Effect of heterogeneous fibers	39
2.5.6. Effect of electrostatic forces	41
2.5.7. Effect of upstream particles concentration.....	43
2.5.8. Effect of temperature	45
2.6. Standards for the filter performance evaluation and the limitations	47
2.7. Filtration of nanoparticles applied in general ventilation	50

Chapter 3: EXPERIMENTAL METHOD AND SYSTEM CALIBRATION	56
3.1. Experimental design.....	56
3.1.1. Setup configuration.....	56
3.1.2. Particle generation system	58
3.1.3. Measurement devices	58
3.2. Penetration measurement	59
3.3. Test procedure.....	60
3.4. Setups characterization (Calibration).....	61
3.4.1. Velocity homogeneity	62
3.4.2. Stabilization test.....	67
3.4.3. Aerosol homogeneity	67
Chapter 4: RESULTS AND DISCUSSION	70
4.1. Introduction.....	70
4.2. Repeatability	70
4.3. Penetration comparison between small setup and big loop setup	71
4.4. Effect of velocity in small setup	74
Chapter 5: CONCLUSIONS AND FUTURE WORK.....	77
5.1. Conclusions.....	77
5.2. Recommendations and Future Work.....	78
REFERENCES	79

LIST OF FIGURES

Figure 2-1: Particles size spectrum for each capture mechanism in aerosol filtration.....	5
(Zhu et al., 2017).....	5
Figure 2-2: Theoretical evolution of the penetration as a function of temperature.....	47
(Mouret et al., 2011)	47
Figure 2-3: Measured collection efficiencies for 9 filters (MERV 6, 7, 8, 10, 11, 12, 13, 14, 16) (Hecker & Hofacre, 2008)	53
Figure 3-1: Schematic of a) the small setup; b) the big loop setup, used to challenge mechanical filters against poly-disperse NPs	57
Figure 3-2: Generation system: 6-jet and 24-jet Collision Nebulizer	58
Figure 3-3: Electrostatic classifier (EC) (left) and condensation particle counter (CPC) (right).....	59
Figure 3-4: Photograph of the tested filter (MERV 8) filter	60
Figure 3-5: Sampling grid with nine-area points for measuring the uniformity of air velocity for small setup (ASHRAE, 2007)	63
Figure 3-6: Sampling grid with nine-area points for measuring the uniformity of air velocity for big loop setup (ASHRAE, 2007)	63
Figure 3-7: Mean of the velocity (m/s) uniformity tests at three configurations in the Small setup.....	64
Figure 3-8: Mean of the velocity (m/s) uniformity tests at three configurations in the Big Loop setup....	65
Figure 3-9: Velocity measurement at center of the upstream according to motor’s characteristic – Linear regression Left) for small setup; Right) for big loop setup	66
Figure 3-10: Mean of the aerosol homogeneity tests at three configurations in the Small setup.....	68
Figure 3-11: Mean of the aerosol homogeneity tests at two configurations in the Big Loop setup.....	69
Figure 4-1: Comparison of penetration data through MERV 8 for both small setup and big loop setup at two constant velocities: 0.75 and 1 m/s. The error bars represent the standard deviations	71
Figure 4-2: Complete procedure to compare the penetration data through MERV 8 for both small setup and big loop setup	73
Figure 4-3: Comparison of penetration data through MERV 8 for both small setup and big loop.....	74
Figure 4-4: Effect of particle size and face velocity on initial particle penetration through MERV 8, in small setup. The error bars represent the standard deviations	75

LIST OF TABLES

Table 2-1: Single fiber efficiency due to diffusion	9
Table 2-2: Single fiber efficiency due to interception.....	13
Table 2-3: Single fiber efficiency due to interception of diffused particles	15
Table 2-4: Single fiber efficiency due to image force.....	16
Table 2-5: Single fiber efficiency due to polarization force.....	18
Table 2-6: Single fiber efficiency due to Coulomb force.....	19
Table 2-7: Dimensionless drag coefficient.....	23
Table 2-8: Models of pressure drop for clogged flat fibrous media.....	26
Table 2-9: Kozeny’s constant relationships	30
Table 2-10: Particle counters size range boundaries (ASHRAE, 2007).....	48
Table 2-11: Minimum Efficiency Reporting Value (MERV) parameters (ASHRAE, 2007)	49
Table 2-12: Overview of Experimental Studies on Nanoparticle Filtration Using Entire Filters	51
(Brochot et al., 2018)	51
Table 3-1: Summary of experimental measurements.....	61

LIST OF ABBREVIATIONS

Abbreviation

Description

ASHRAE	American Society of Heating, Refrigerating, and Air-Conditioning Engineers
ANSI	American National Standards Institute
CV	Coefficient of Variation
CPC	Condensation Particle Counter
DMA	Differential Mobility Analyzer
EC	Electrostatic Classifier
HVAC	Heating, Ventilating and Air-conditioning
HEPA	High-Efficiency Particulate Air
MPPS	Most Penetrating Particle Size
MERV	Minimum efficiency reporting value
NaCl	Sodium Chloride
NIOSH	National Institute for Occupational Safety and Health
NPs	Nano-Particles
RH	Relative Humidity
SMPS	Scanning Mobility Particle Sizer
UFP	Ultra-Fine Particle

LIST OF SYMBOLS

English Symbols

Description

a	Contact radius (m)
a_g	Particle specific area (m^{-1})
C_d	Gas slip correction factor for diffusion (-)
C_r	Gas slip correction factor for interception (-)
$C_{\dot{a}}$	Correction factor to lower the efficiency for diffusion (-)
C_c	Cunningham correction factor (-)
Co	Overlap parameter (-)
C_T	Drag coefficient for a fiber (-)
$C_{Tm}(l, t)$	Drag coefficient for a fiber loaded with particles (-)
D	Diffusion coefficient ($m^2 \cdot s^{-1}$)
D_n	Diffusion coefficient of neutral nanoparticles ($m^2 \cdot s^{-1}$)
d_p	Particle diameter (m)
d_m	Particle mobility diameter (m)
d_g	Gas molecule diameter (m)
\bar{d}_p	Mean particle diameter (m)
d_f	Fiber diameter (m)
d_{agg}	Aggregated or agglomerated particle size (m)
d_{pG}	Count median diameter (m)
d_{vg}	Geometric mean size of the volume equivalent diameter (m)
d_{eq}	Pore diameter (m)
$d_{fm}(l, t)$	Diameter of the fiber loaded with particles (m)
E	Electric field ($V \cdot m^{-1}$)
E_{Σ}	Total single fiber efficiency (-)
E_m	Single fiber efficiency due to mechanical mechanism (-)
E_D	Single fiber efficiency due to diffusion (-)
E_R	Single fiber efficiency due to interception (-)
E_{DR}	Single fiber efficiency due to interception of diffused particles (-)
E_I	Single fiber efficiency due to impaction (-)
E_e	Single fiber efficiency due to electrostatic mechanism (-)
E_{IM}	Single fiber efficiency due to image force (-)
E_P	Single fiber efficiency due to polarization force (-)
E_C	Single fiber efficiency due to columbic force (-)
e	Elementary charge ($1.602 \times 10^{-19} C$)
F	Drag coefficient (-)
h_k	Kozeny constant (-)
H_{Fan}	Hydrodynamic factor for the "fan" model (-)
H_{Ku}	Hydrodynamic factor according to Kuwabara (-)
H_{La}	Hydrodynamic factor according to Lamb (-)
k	Media penetration factor (-)
Kn_f	Fiber Knudsen number (-)
Kn_p	Particle Knudsen number (-)
K_b	Boltzmann constant ($1.381 \times 10^{-23} J \cdot K^{-1}$)
L	Medium thickness (m)
L^*	Medium corrected thickness (m)
L_f'	Total length of fibers per unit volume (m^{-2})
L_p'	Length of the chain of particles per unit volume (m^{-2})

m	Particle mass (kg)
M_p	Molecular weight of nanoparticle (kg. mol^{-1})
M_g	Molecular weight of carrier gas (kg. mol^{-1})
N	Number concentration of gas molecules ($\#/m^3$)
n	Number of elementary charges (-)
Pe	Peclet number (-)
q	Charge carried by particle (C)
Q_f	Quality factor (-)
R	Interception parameter (-)
Re_f	Fiber Reynolds number (-)
T	Absolute temperature (K)
U_0	Face velocity (m.s^{-1})
U	Flow velocity inside the medium (m.s^{-1})
v	Velocity of gas molecule (m.s^{-1})
\bar{v}_r	Root mean square velocity of gas (m.s^{-1})
Z_p	Electrical mobility of particle ($\text{m}^2 \cdot \text{s}^{-1} \cdot \text{V}^{-1}$)

Greek Symbols

α_f	Packing density of medium (-)
α_p	Packing density of collected particles (-)
α_{pc}	Particle deposit (cake) packing density (-)
β	Size dependent parameter (-)
ϵ_0	Permittivity of vacuum ($8.84 \times 10^{-12} \text{F. m}^{-1}$)
ϵ_p	Particle dielectric constant (-)
ϵ_f	Fiber dielectric constant (-)
μ	Air dynamic viscosity (Pa.s)
κ	Dynamic shape factor of particles (-)
η	Filtration efficiency (-)
λ	Mean free path of gas molecules (m)
λ_q	Linear charge of fiber (C.m^{-1})
ρ_p	Particle density (kg.m^{-3})
$v(\alpha_{pc})$	Void function (-)
σ_g	Geometric standard deviation of particle size distribution (-)
Ω	Filtration area (m^2)
Δp	Pressure drop (Pa)
Δp_0	Pressure drop of clean medium (Pa)

Description

Chapter 1: INTRODUCTION

1.1. Background

Nanoparticles are ultra-fine particles (UFPs) with diameters smaller than or equal to 100 nm. These particles have many major health and safety challenges because of their size. Exposure to these nanoscale materials has harmful effects on human health (Borm & Kreyling, 2004; Kreyling et al., 2004; Mills et al., 2009; Oberdörster, 2010). There are several nanoparticle sources (combustion, mobile emissions, atmospheric conversion, industrial processes or production of nanoparticles) and they can be found in outdoor and indoor pollution. Filtration is the primary and most effective solution to protect exposed people. Furthermore, the penetration of nanoparticles was not clearly understood because of the difficulties of set - up system and measurement of penetration. Accordingly, with the rapid expansion in the manufacturing area of nano-products, a method must be developed for measuring the effectiveness of mechanical filters used in general ventilation systems. To our information, there is no current standard for quantifying or classifying these filters' performance against NPs.

1.2. Research Objective

The main objective of this study was to develop a measurement procedure to evaluate the effectiveness of mechanical filters used in general ventilation systems against (NPs). In this regard, a small setup was designed, build and qualified. Then measurement procedure was validated by comparing the penetration measurements with those obtained on qualified big loop setup, which was inspired by ASHRAE setup for nano-metric particles. One type of mechanical filter rated (MERV 8) in three depth sizes (1, 2 and 4in) was used to illustrate the full penetration range that can be measured on both setups. The achievement of this objective will be done in 3 steps:

- 1- Design and implementation of a small setup and a big loop setup.
- 2- Calibration of the setups according to ASHRAE 52.2 standard.
- 3- Validate the results by measuring the initial penetration of one type of mechanical filter rated (MERV 8) in three depth sizes (1, 2 and 4in) used in ventilation systems by comparing penetration measurements to the standard and to measurements in the both setups.

1.3. Thesis Outline

Chapter 2 explains the fundamentals of nanoparticle filtration and provides critical reviews on the filtration performance of media against NPs. The testing protocol for mechanical filters is also presented. Chapter 3 describes and compares two different experimental setups for challenging one type of mechanical filter rated (MERV 8) in three depth sizes (1, 2 and 4in) used in ventilation systems with NPs. Thereafter, the results of calibration and pre-qualification tests will be presented. Chapter 4 illustrates and discusses the experimental results. Finally, chapter 5 outlines the conclusions and recommendations for future direction.

Chapter 2: LITERATURE REVIEW

2.1. Introduction

Filtration is a process that removes particles from a liquid or gas. The use of filter layers is one of the most efficient processes, and nonwoven fibrous media (glass fibers or synthetic fibers, for example) are the most frequently used to capture particles and reduce indoor exposure. Filtration by means of personal protective equipment or general ventilation is widely used for worker protection and environmental protection. However, filters are not chosen solely on the basis of their ability to collect particles: sources of pollution, operating conditions, energy cost, maintenance requirements and service life must also be taken into account.

To characterize the performance of a fibrous medium, two parameters are used: filtration efficiency (η) and pressure drop (Δp). These two parameters are related to the geometric characteristics of the medium, the particle's characteristics and the operating conditions (e.g. filtration velocity, temperature, humidity); hence the first and foremost task is to study the interactions between these three aspects. Media are defined as porous structures composed of a tangle of fibers (e.g. glass, cotton or polyester) with a preferred orientation across the direction of gas flow. They are capable of efficiently removing sub-micrometer particles from gas streams with low pressure drop due to their low packing density, i.e., the ratio of the total volume of all fibers in the medium to the volume of the medium (α_f is in the range of 1-30%). Fibers can be produced from a wide range of materials, such as polymers, glass, plastics or metals, and they are used in many applications including respirators, industrial gas cleaning, vacuum cleaners, cleanrooms, air purification systems and indoor air purifiers.

2.2. Filtration capture mechanisms

As an aerosol stream approaches a fiber, particles may deposit on the fiber due to several mechanisms such as gravitational settling, inertial impaction, interception, diffusion and electrostatic forces.

The first four are known as mechanical mechanisms. The gravitational settling is less important for most particle sizes due to the fact that the filtering contribution of the gravitational force appears to be minimal. Gravity sedimentation can be completely neglected if size of the particles are smaller than $0.5\mu\text{m}$ (Zhu et al., 2017). Inertial impaction occurs when a particle, by its inertia, departs from the initial gas streamline and hits a fiber. Interception turns up because a particle has a finite size and starts to deposit when it comes within one particle radius of the fiber surface. For particles smaller than $0.1\mu\text{m}$, diffusion can be forceful enough to move them from the original streamlines to the fiber due to the random motion of the particles (Mostofi et al., 2010). Electrostatic forces appear when particles or fibers carry electric charges or when an external electric field is applied to the medium. There are several different types of electrostatic forces (C. Wang, 2001). The most important one is Coulomb force, which is an interaction between a charged particle and a unipolar or bipolar charged fiber such as those in an electret fibrous medium. Other electrostatic forces include image and polarization forces, which are defined as interactions between a charged particle and a neutral fiber, or a charged fiber and a neutral particle, respectively.

Figure 1 illustrates the particles size spectrum for each capture mechanism. Generally, diffusion plays a crucial role for particles smaller than $0.1\mu\text{m}$, interception is dominant capture mechanism for particles in the range of $0.1\text{-}1\mu\text{m}$, whereas inertial impaction is effective capture mechanism

for particles larger than 0.3-1 μm . Meanwhile the electrostatic forces are typically useful for improving the collection of particles in the range of 0.15- 0.5 μm (Zhu et al., 2017).

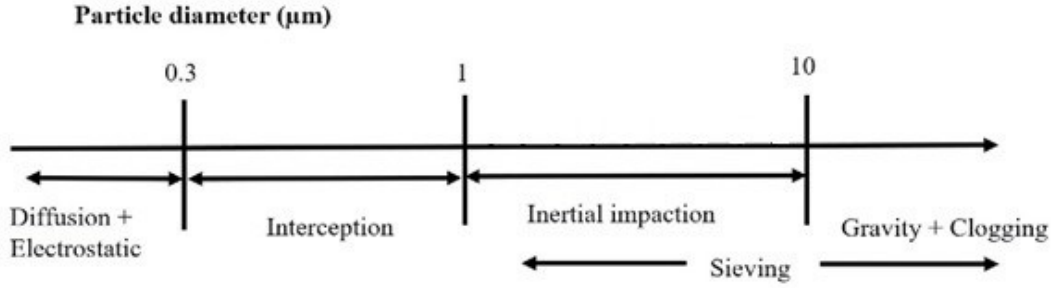


Figure 2-1: Particles size spectrum for each capture mechanism in aerosol filtration (Zhu et al., 2017)

2.2.1. Initial filtration efficiency of fibrous media

The initial filtration efficiency (η) of a medium is considered to be a function of total single fiber efficiency (E_{Σ}), and is given as (Hinds, 1999):

$$\eta = 1 - \exp \left[\frac{-4\alpha_f E_{\Sigma} L}{\pi d_f (1 - \alpha_f)} \right] \quad (2-1)$$

where α_f is the packing density of the medium, L is the thickness of the medium, and d_f is the fiber diameter. Single fiber efficiency is the ratio of the number of settled particles to the unit length of fiber surface perpendicular to the airflow. It is based on all the separate deposition mechanisms and thus overestimates the overall efficiency, since captured particles may be counted more than once. E_{Σ} is given by (Lathrache & Fissan, 1987; Tennal et al., 1991):

$$E_{\Sigma} = 1 - (1 - E_m)(1 - E_e) \quad (2-2)$$

where E_m is the single fiber efficiency due to mechanical mechanisms

$$E_m = 1 - (1 - E_D)(1 - E_R)(1 - E_{DR})(1 - E_I) \quad (2-3)$$

and E_e is the total single fiber efficiency due to electrostatic mechanisms.

$$E_e = 1 - (1 - E_{IM})(1 - E_P)(1 - E_C) \quad (2-4)$$

where E_D and E_R are due to diffusion and interception (K. Lee & Liu, 1982); E_I is due to impaction (Hinds, 1999), E_P is due to polarization force; E_C is due to Columbic force (Lathrache & Fissan, 1987; Tennal et al., 1991), and E_{IM} is due to image force (Kanaoka et al., 1987). The equation for total single fiber efficiency is an approximation based on the assumption that all separate filtration mechanisms are independent if all of them are much smaller than unity (Brown, 1993; Kasper et al., 1978; K. Lee & Liu, 1982; Payet et al., 1992). In such a case it will be considered that total single fiber efficiency (E_Σ) is given by the sum of the efficiencies for each of the individual mechanisms, plus an additional term (E_{DR}) indicating the interception of the particles undergoing diffusion.

The application of this term to elongated particles is unclear.

$$E_\Sigma \cong E_D + E_I + E_{DR} + E_R + E_P + E_C + E_{IM} \quad (2-5)$$

Finally, the dominant mechanism in nanoparticle filtration especially for particles smaller than 20nm is diffusion, and the effects of other mechanisms are negligible (Mostofi et al., 2010). As a result, the total single fiber efficiency is given as:

$$E_\Sigma \cong E_D \quad (2-6)$$

All the single fiber efficiency expressions for the fibrous media due to diffusion, interception, interception of diffused particles and electrostatic forces are given in Tables 2-1 to 2-6

Single fiber efficiency due to diffusion is a function of the Peclet number (Pe), which is given as:

$$Pe = \frac{d_f U}{D} \quad (2-7)$$

where

$$U = \frac{U_0}{(1-\alpha_f)} \quad (2-8)$$

where U_0 is the face velocity (defined as flow velocity at the medium face), U is the flow velocity through the medium, d_f is the fiber diameter, α_f is the medium packing density and D is the diffusion coefficient, and it is given by (Hinds, 1999):

$$D = \frac{K_b T C_c}{3\pi\mu d_p} \quad (2-9)$$

where K_b is the Boltzmann's constant 1.38×10^{-23} J/K, T is the absolute temperature, μ is the air viscosity, d_p is the particle diameter and C_c is the Cunningham correction factor, which expresses the non-continuum interaction between the particles and the carrier gas. Nanoparticles are small enough to approach the mean free path of a gas under normal conditions; the Cunningham correction factor is used to consider the slip condition in the gas flow, and it is defined by (M. D. Allen & Raabe, 1985):

$$C_c = 1 + Kn_p \left[1.257 + 0.4 \exp\left(-\frac{1.1}{Kn_p}\right) \right] \quad (2-10)$$

where Kn_p is the particle Knudsen number, which is defined by:

$$Kn_p = \frac{2\lambda}{d_p} \quad (2-11)$$

where λ is the mean free path of the gas. The Knudsen number is used for demonstrating the validation of the flow continuity assumption in the Navier-Stokes equation. For nanoparticles, the assumption of the continuum flow fails and the flow becomes a free molecular, which means that the nanoparticle diameter is much smaller than the mean free path of the molecules. Under these conditions, each molecule travels the length scale of the nanoparticle a number of times before colliding with other molecules (Przekop & Gradoń, 2008). The diffusion coefficient of a neutral nanoparticle between 0.5 and 2nm in size is given by (Loeb, 1961):

$$D_n = \frac{3.26\bar{v}_r}{3\pi N(d_p+d_g)^2} \sqrt{1 + \frac{M_g}{M_p}} \quad (2-12)$$

where \bar{v}_r is the root mean square velocity of the gas (502 m/s at STP), d_g is the gas molecule diameter (0.37nm), N is the number concentration of gas molecules ($2.45 \times 10^{25} /m^3$ at STP), M_g is the molecular weight of the carrier gas (28.96 for air at STP), and M_p is the molecular weight of the nanoparticles. The molecular weight of the air molecules is much less than that of the particles, so that the square root term can be ignored (Ichitsubo et al., 1996). For singly charged nanoparticles the diffusion coefficient can be estimated by the following equation (Ichitsubo et al., 1996):

$$D = \frac{D_n}{\frac{0.402e^2(d_g)^3}{1 + \frac{2K_b T(d_p + d_g)^4}{2K_b T(d_p + d_g)^4}}} \quad (2-13)$$

Table 2-1: Single fiber efficiency due to diffusion

Expression	Remarks		Ref.
$E_D = 1.7H_{La}^{-1/3}Pe^{-2/3}$	<ul style="list-style-type: none"> • $Re_f = \frac{\rho U d_f}{\mu}$ • $H_{La} = 2 - \ln Re_f$ 	<ul style="list-style-type: none"> • Theoretical model 	(Langmuir, 1942)
$E_D = 2.9H_{La}^{-1/3}Pe^{-2/3}$	<ul style="list-style-type: none"> • $Re_f = \frac{\rho U d_f}{\mu}$ • $H_{La} = 2 - \ln Re_f$ 	<ul style="list-style-type: none"> • Theoretical model 	(Natanson, 1957)
$E_D = 2.27H_{Ku}^{-1/3}Pe^{-2/3}(1 + 0.62Kn_fPe^{1/3}H_{Ku}^{-1/3})$	<ul style="list-style-type: none"> • $H_{Ku} = -\frac{1}{2}\ln\alpha_f - \frac{3}{4} - \frac{1}{4}\alpha_f^2 + \alpha_f$ • $Kn_f = \frac{2\lambda}{d_f}$ 	<ul style="list-style-type: none"> • In good agreement for particles $d_p > 20nm$ 	(Pich, 1965)
$E_D = 2.9H_{Ku}^{-1/3}Pe^{-2/3} + 0.624Pe^{-1}$	<ul style="list-style-type: none"> • $Pe \gg 1$ • $Re_f \ll \alpha_f^{1/2}$ • $\alpha_f \ll 1$ 	<ul style="list-style-type: none"> • Analysis of boundary layer 	(Stechkina & Fuchs, 1966)
$E_D = 2.9H_{Ku}^{-1/3}Pe^{-2/3}$	<ul style="list-style-type: none"> • $\alpha_f < 0.1$ • $Pe > 2$ • $R \ll 1$ 	<ul style="list-style-type: none"> • Theoretical model • For parallel staggered fibers • High porosity fibrous media 	(Stechkina & Fuchs, 1966)
$E_D = 2.7Pe^{-2/3}$	<ul style="list-style-type: none"> • $0.01 < \alpha_f < 0.15$ 	<ul style="list-style-type: none"> • Empirical model • Continuum flow regime • In good agreement for particles down to 2nm • In good agreement for wire screens 	(A. Kirsch & Fuchs, 1968)
$E_D = 1.5Pe^{-2/3}$			(C. N. Davies, 1973)

$E_D = 3.2(k_1)^{-1/2}(\tau Kn_f)^{1/2}Pe^{1/2}$	<ul style="list-style-type: none"> • $10^{-2} < Kn_f < 10^{-1}$ • $k_1 = H_{Ku} + \xi Kn_f$ • $\delta_1 = \left(\frac{2k_1}{Pe}\right)^{1/3} < Kn_f$ • $Pe \cong 1$ 	<ul style="list-style-type: none"> • Slip flow regime • δ_1 is the length characteristic of boundary layer and ξ is a coefficient that is dependent on a gas-fiber interaction and is in the order of unity 	(Kirsh & Stechkina, 1978)
$E_D = 2.7Pe^{-2/3} \left(1 + 0.39H_{FAN}^{-\frac{1}{3}}Pe^{\frac{1}{3}}Kn_f\right) + 0.624Pe^{-1}$	<ul style="list-style-type: none"> • $H_{FAN} = -0.5\ln\alpha_f - 0.52 + 0.46\alpha_f + 1.43(1 - \alpha_f) Kn_f$ 	(A. Kirsch & Zhulanov, 1978a)	
$E_D = 2.6\left(\frac{1 - \alpha_f}{H_{Ku}}\right)^{1/3}Pe^{-2/3}$	<ul style="list-style-type: none"> • Theoretical model • Continuum flow regime • For large Peclet numbers • Underestimates filtration efficiency of nanoparticles for experimental data • Irregularities in fiber direction and non-uniformly distributed fibers are not taken into account 	(K. Lee & Liu, 1982)	
$E_D = 1.6\left(\frac{1 - \alpha_f}{H_{Ku}}\right)^{1/3}Pe^{-2/3}$	<ul style="list-style-type: none"> • Fiber orientations are not orthogonal to the aerosol stream • Heterogeneous fibers • Continuum flow regime • In good agreement for particles $d_p < 0.5\mu m$ • In good agreement for real fibrous media with irregularities in fiber direction and non-uniformly distributed fibers • Underestimates filtration efficiency of nanoparticles for experimental data 	(K. Lee & Liu, 1982)	
$E_D = 2.58\left(\frac{1 - \alpha_f}{H_{Ku}}\right)^{1/3}Pe^{-2/3}$	<ul style="list-style-type: none"> • In good agreement for particles $d_p < 100nm$ • Uncharged • Intermediate value of α 	(K. Lee & Liu, 1982)	
$E_D = 4.89\left(\frac{1 - \alpha_f}{H_{Ku}}\right)^{0.54}Pe^{-0.92}$	<ul style="list-style-type: none"> • $0.029 < \alpha_f < 0.1$ • $Pe < 50$ 	<ul style="list-style-type: none"> • Theoretical model 	(Rao & Faghri, 1988)
$E_D = 1.8\left(\frac{1 - \alpha_f}{H_{Ku}}\right)^{1/3}Pe^{-2/3}$	<ul style="list-style-type: none"> • $0.029 < \alpha_f < 0.1$ • $100 < Pe < 300$ • $0.26 < Re_f < 0.31$ 	<ul style="list-style-type: none"> • Theoretical model 	(Rao & Faghri, 1988)

$E_D = 1.6 \left(\frac{1 - \alpha_f}{H_{Ku}} \right)^{1/3} Pe^{-2/3} C_d$	<ul style="list-style-type: none"> • $10^{-2} < Kn_f < 10^{-1}$ • $C_d = 1 + 0.388 Kn_f \left[\frac{(1 - \alpha_f) Pe}{H_{Ku}} \right]^{1/3}$ 	<ul style="list-style-type: none"> • Slip flow regime • Overestimates filtration efficiency of nanoparticles for experimental data • In good agreement for real fibrous media with irregularities in fiber direction and non-uniformly distributed fibers • Filtration efficiency of nanoparticles is greater than unity with a low Peclet number 	<p>(B. Y. Liu & Rubow, 1990)</p>
$E_D = 1.6 \left(\frac{1 - \alpha_f}{H_{Ku}} \right)^{1/3} Pe^{-2/3} C_d C_{d'}$	<ul style="list-style-type: none"> • $10^{-2} < Kn_f < 10^{-1}$ • $C_{d'} = \left[1 + 1.6 \left(\frac{1 - \alpha_f}{H_{Ku}} \right)^{1/3} Pe^{-2/3} C_d \right]^{-1}$ • $0.02 < d_p < 0.5 \mu m$ • $d_f = 1 \mu m$ and $\alpha_f = 0.08$ 	<ul style="list-style-type: none"> • Slip flow regime • Liquid aerosol • Correction factor ($C_{d'}$) modified the Lee and Liu equation in order to lower the efficiency value to less than unity • Slightly overestimates filtration efficiency of nanoparticles if the mean fiber diameter is considered • In good agreement with experimental data, if a resistance-equivalent diameter of the fiber is considered • In good agreement for real fibrous media with irregularities in fiber direction and non-uniformly distributed fibers 	<p>(Payet et al., 1992)</p>

$E_D = 2Pe^{-2/3}$	<ul style="list-style-type: none"> • Continuum flow regime • Not accurate, especially for nanoparticles 		(Hinds, 1999)
$E_D = 0.84Pe^{-0.43}$	<ul style="list-style-type: none"> • $10^{-2} < Kn_f < 10^{-1}$ 	<ul style="list-style-type: none"> • Slip flow regime • In good agreement with the equation predicted by Stechkina (1966) if $Pe > 100$ • In good agreement with the equation predicted by Krish and Stechkina (1978) if $Pe \cong 1$ • In good agreement for all ranges of Peclet numbers • Mean fiber diameter is considered • In a good agreement for real fibrous media conditions 	(J. Wang et al., 2007)

Table 2-2: Single fiber efficiency due to interception

Expression	Remarks		Ref
$E_R = 2.9\alpha_f^{1/3}R^{1.75}$	<ul style="list-style-type: none"> $R = \frac{d_p}{d_f}$ (Interception parameter) 	<ul style="list-style-type: none"> Continuum flow regime Theoretical model 	(Kuwabara, 1959)
$E_R = \frac{(1+R)^{-1} - (1+R) + 2(1+1.996Kn_f)(1+R)\ln(1+R)}{2(-0.75 - 0.5\ln\alpha_f) + 1.996Kn_f(-0.5 - \ln\alpha_f)}$	<ul style="list-style-type: none"> No slip flow at gas-fiber interface In good agreement for particles $d_p > 20nm$ 		(Pich, 1966)
$E_R = \frac{1+R}{2H_{Ku}} \left[2\ln(1+R) - 1 + \left(\frac{1}{1+R}\right)^2 \right]$	<ul style="list-style-type: none"> Continuum flow regime 		(Stechkina et al., 1969)
$E_R = \frac{1+R}{2H_{Ku}} \left[2\ln(1+R) - 1 + \alpha_f + \left(\frac{1}{1+R}\right)^2 \left(1 - \frac{\alpha_f}{2}\right) - \frac{\alpha_f}{2}(1+R)^2 \right]$	<ul style="list-style-type: none"> Continuum flow regime Spherical particles 		(Kirsh & Stechkina, 1978)
$E_R = \frac{1+R}{2H_{FAN}} \left[2\ln(1+R) - 1 + \left(\frac{1}{1+R}\right)^2 + \frac{2.86(2+R)R}{(1+R)^2} Kn_f \right]$	<ul style="list-style-type: none"> Slip flow regime 		(A. Kirsch & Zhulanov, 1978b)
$E_R = \left(\frac{1-\alpha_f}{H_{Ku}}\right) R^2 (1+R)^{\frac{-2}{3(1-\alpha_f)}}$	<ul style="list-style-type: none"> Continuum flow regime 		(K. W. Lee & Gieseke, 1979)
$E_R = \left(\frac{1-\alpha_f}{H_{Ku}}\right) \frac{R^2}{1+R}$	<ul style="list-style-type: none"> $R < 0.2$ $\alpha_f < 0.5$ 	<ul style="list-style-type: none"> Continuum flow regime Irregularities in fiber direction and non-uniformly distributed fibers are not taken into account 	(K. Lee & Liu, 1982)

$E_R = 0.6 \left(\frac{1 - \alpha_f}{H_{Ku}} \right) \frac{R^2}{1 + R}$	<ul style="list-style-type: none"> • $1 < U < 30 \text{ cm/s}$ • $0.05 < d_p < 1.3 \mu\text{m}$ • $0.0045 < R < 0.12$ • $0.0086 < \alpha_f < 0.151$ 	<ul style="list-style-type: none"> • Continuum flow regime • Fibers are not perpendicular to flow direction and are not uniformly distributed • Continuum flow regime • In good agreement for particles $d_p < 0.5 \mu\text{m}$ • Underestimates filtration efficiency of nanoparticles for experimental data • In good agreement for real fibrous media with irregularities in fiber direction and non-uniformly distributed fibers 	<p>(K. Lee & Liu, 1982)</p>
$E_R = \frac{R(R + 1.996Kn_f)}{H + 1.996Kn_f(H + R)}$	<ul style="list-style-type: none"> • $H = -0.7 - 0.5 \ln(\alpha_f)$ 	<ul style="list-style-type: none"> • Slip flow regime 	<p>(Matteson, 1987)</p>
$E_R = 2.4 \alpha_f^{1/3} R^{1.75}$	<ul style="list-style-type: none"> • Continuum flow regime 	<p>(Miecret & Gustavsson, 1989)</p>	
$E_R = 0.6 \left(\frac{1 - \alpha_f}{H_{Ku}} \right) \frac{R^2}{1 + R} C_r$	<ul style="list-style-type: none"> • $C_r = 1 + \frac{1.996Kn_f}{R}$ • $0.005 < d_p < 1 \mu\text{m}$ • $Kn_f \cong 1$ 	<ul style="list-style-type: none"> • Slip flow at gas-fiber interface • Discontinuity of fluid around fibers • Slightly overestimates filtration efficiency of nanoparticles if mean fiber diameter is considered • Overestimates filtration efficiency of nanoparticles for experimental data • In good agreement with experimental data, if a resistance-equivalent diameter of the fiber is considered • In good agreement for real fibrous media with irregularities in fiber direction and non-uniformly distributed fibers 	<p>(B. Y. Liu & Rubow, 1990; Payet et al., 1992)</p>

Table 2-3: Single fiber efficiency due to interception of diffused particles

Expression	Remarks		Ref
$E_{DR} = \frac{1.6Ka^{1/3}Pe^{-2/3}(1 + 0.388Ka^{1/3}Pe^{1/3}Kn_f)}{1 + 1.6Ka^{1/3}Pe^{-2/3} + 0.6211.6Ka^{2/3}Pe^{-1/3} + 0.6Ka\frac{R^2}{1+R}\left(1 + \frac{1.999Kn_f}{R}\right)}$	<ul style="list-style-type: none"> • $Ka = \frac{(1-\alpha_f)}{H_{Ku}}$ • $10^{-2} < Kn_f < 10^{-1}$ 	<ul style="list-style-type: none"> • Slip flow at gas-fiber interface 	(Payet et al., 1992)
$E_{DR} = \frac{1.24R^{2/3}}{(H_{Ku}Pe)^{1/2}}$	<ul style="list-style-type: none"> • $H_{Ku}/Pe < 0.024$ • $R < 0.5$ 	<ul style="list-style-type: none"> • Spherical particles 	(Hinds, 1999)

Table 2-4: Single fiber efficiency due to image force

Expression	Remarks		Ref
$E_{IM} = 1.5N_{0q}^{1/2}$	<ul style="list-style-type: none"> • $N_{0q} = \left(\frac{\epsilon_f - 1}{\epsilon_f + 1}\right) \frac{q^2 C_c}{12\pi^2 \mu U \epsilon_0 d_p d_f^2}$ • $q = n \times e$ • $n =$ Number of elementary charges • $e = 1.6 \times 10^{-19} C$ • $\epsilon_f =$ Fiber dielectric constant • $\epsilon_0 =$ vacuum permittivity $= 8.84 \times 10^{-12} Fm^{-1}$ • $N_{0q} > 10^{-5}$ • $0.1\mu m < d_p < 1\mu m$ 	<ul style="list-style-type: none"> • 320 elementary charges per particle • Mean number of charges characterizing charge distribution instead of defined number of charges 	(Lundgren & Whitby, 1965)
$E_{IM} = 2.3N_{0q}^{1/2}$	<ul style="list-style-type: none"> • $N_{0q} > 10^{-5}$ • $0.1\mu m < d_p < 1\mu m$ 	<ul style="list-style-type: none"> • 320 elementary charges per particle • Mean number of charges characterizing charge distribution instead of defined number of charges 	(Yoshioka et al., 1968)
$E_{IM} = 1.48N_{0q}^{0.93}$	<ul style="list-style-type: none"> • $10^{-4} < N_{0q} < 10^{-2}$ 		(Otani et al., 1993)

$E_{IM} = 0.51H_{Ku}^{-0.35}N_{0q}^{0.73}$	<ul style="list-style-type: none"> • $10^{-2} < N_{0q} < 1$ 	(Otani et al., 1993)
$E_{IM} = 0.54H_{Ku}^{-0.60}N_{0q}^{0.40}$	<ul style="list-style-type: none"> • $1 < N_{0q} < 100$ 	(Otani et al., 1993)
$E_{IM} = 9.7N_{0q}^{1/2}$	<ul style="list-style-type: none"> • $N_{0q} > 10^{-5}$ 	(Alonso et al., 2007)
$E_{IM} = 29.7N_{0q}^{0.59}$	<ul style="list-style-type: none"> • $10^{-7} < N_{0q} < 10^{-5}$ • $25nm < d_p < 65nm$ 	<ul style="list-style-type: none"> • Carrying definite charges of 0, +1, +2 and +3 elementary charges • Transition regime (Alonso et al., 2007)

Table 2-5: Single fiber efficiency due to polarization force

Expression	Remarks	Ref
$E_p = \left(\frac{3\pi}{2}\right)^{1/3} N_{q0}^{0.75}$		
$E_p = 0.84N_{q0}^{1/2}$	<ul style="list-style-type: none"> • $N_{q0} = \left(\frac{\epsilon_p - 1}{\epsilon_p + 2}\right) \frac{\lambda_q^2 d_p^2 c_c}{3\pi^2 \mu U \epsilon_0 d_f d_f^3}$ λ_q = linear charge of fiber ϵ_p = particle dielectric constant ϵ_0 = vacuum permittivity = $8.84 \times 10^{-12} F/m$ • $\alpha_f < 0.03$ • $0.03 < N_{q0} < 0.91$ 	<p>(Kraemer & Johnstone, 1955; Stenhouse, 1974)</p>

Table 2-6: Single fiber efficiency due to Coulomb force

Expression	Remarks	Ref
$E_C = \pi N_{qq}$	<ul style="list-style-type: none"> • $N_{qq} = \frac{\lambda_q q C_c}{3\pi^2 \mu U \epsilon_0 d_p d_f} = \lambda_q \frac{Z_p}{U \epsilon_0 d_f}$ $q = n \times e =$ charge carried by particle $n =$ number of elementary charges $e = 1.6 \times 10^{-19} C$ $\lambda_q =$ linear charge of fiber $Z_p =$ electrical mobility of particle 	(Kraemer & Johnstone, 1955)
$E_C = 0.78 N_{qq}$	<ul style="list-style-type: none"> • $10^{-3} < N_{qq} < 10^{-1}$ 	(Otani et al., 1993)
$E_C = 0.59 H_{Ku}^{-0.17} N_{qq}^{0.83}$	<ul style="list-style-type: none"> • $10^{-1} < N_{qq} < 10$ 	(Otani et al., 1993)

Several experiments have been carried out to validate the possibility of using the theoretical and empirical models (Tables 2-1 to 2-6) to calculate nanoparticle filtration efficiency.

In conclusion, each theoretical and empirical equation is best used in a particular condition related to the specific characteristics of the media and particles, but none are accurate enough for use with a wide range of particles and fibrous media parameters.

Another strategy to calculate single fiber efficiency is following the path of a particle till collapse on the fiber surface. The Langevin equation is applied to demonstrate the motion of nanoparticles, and a Brownian dynamics algorithm is used to integrate the Langevin equation in order to measure the single fiber efficiency. A full explanation of this algorithm is available (Bałazy & Podgórski, 2007).

2.2.2. Filtration efficiency of clogged fibrous media

During use of a medium, its efficiency decreases over time due to the clogging of fibrous media. This stage in the medium's life – dynamic filtration – involves changes in the medium's properties over time, as particle deposition increases. Efficiency is thus a function of time (Mahdavi et al., 2015).

Classical models of single fiber efficiency (Tables 2-1 to 2-6) are used to determine the initial filtration efficiency of a fibrous filter (Eq. 2-1). These models are based on the structural properties of the medium. A new model for the clogged medium was proposed by (Hinds & Kadrichu, 1997) and (Kirsch, 1998) based on the increase in two parameters: the mean diameter of the fibers and the packing density of the medium with an increase in number of collected particles. According to Hinds and Kadrichu, the new packing density (α) and the new mean fiber diameter (d_f^*) of a depth-clogged medium are given by:

$$\alpha = \alpha_f + \alpha_p \quad (2-14)$$

$$d_f^* = \frac{d_f L_f' + d_p L_p'}{L_f' + L_p'} \quad (2-15)$$

where L_f' is the total length of the fibers per unit volume and L_p' is the length of the chain of particles per unit volume.

$$L_f' = \frac{4\alpha_f}{\pi d_f^2} \quad (2-16)$$

and

$$L_p' = N d_p L_T \quad (2-17)$$

Where N is the number of collected particles per unit volume and L_T is the relative length of the chains of particles with respect to the fibers. Based on this model the medium is compared to a new medium with different characteristics. This approach can translate the evolution of the medium efficiency during clogging.

2.3. Pressure drop of flat fibrous media

2.3.1. Pressure drop of clean flat fibrous media

Several relations have been proposed to measure the pressure drop across clean fibrous media.

Most of them are according to Darcy's law and given as:

$$\Delta p_0 = \mu U_0 L_f F \quad (2-18)$$

where μ is the gas dynamic viscosity, U_0 the face velocity, F the drag coefficient, and L_f the length of all fibers per unit of medium area. The total length of the fiber is linked to the medium thickness L and the fiber diameter d_f , which is given as:

$$L_f = \frac{4\alpha_f L}{\pi d_f^2} \quad (2-19)$$

Combining the two equations gives the results as:

$$\Delta p_0 = \frac{4\mu\alpha_f U_0 L}{\pi d_f^2} F \quad (2-20)$$

Different models of the dimensionless drag coefficient F are summarized in Table 2-7. The approaches of Happel (Happel, 1959), Kuwabara (Kuwabara, 1959), Fuchs (Fuchs & Stechkina, 1963), and Pich (Pich, 1966) were based on a theoretical calculation for a viscous flow perpendicular to an array of parallel cylinders. The approaches of Davies (Davies, 1953), Chen (Chen, 1955), Spielman (Spielman & Goren, 1968), Henry (Henry & Ariman, 1983) and Jackson (Jackson & James, 1986), on the other hand, were based on a theoretical calculation for a viscous flow across a random arrangement of fibers. Discrepancies between the pressure drops predicted by these models and the experimental measurements (Davies, 1953) were noted, mainly due to the fact that real fibrous media do not have the regular geometry assumed in the theoretical model. The empirical model suggested by (Davies, 1953), which has been tested for a large amount of experimental data, is the most generally used.

Table 2-7: Dimensionless drag coefficient

Expressions for F	Remarks	Ref.
$F = \frac{4\pi}{\left(-\ln\alpha_f - \frac{3}{2} + 2\alpha_f - \frac{\alpha_f^2}{2}\right)}$	Flow is parallel to fibers	(Langmuir et al., 1942)
$F = 16\pi\alpha_f^{1/2}(1 + 56\alpha_f^3)$ $F = 16\pi\alpha_f^{1/2}$	Random arrangement of fibers Empirical model $0.006 < \alpha_f < 0.3$ $0.006 < \alpha_f$	(C. Davies, 1953)
$F = \frac{4C_2}{\ln(C_1\alpha_f^{-\frac{1}{2}})(1 - \alpha_f)}$	Random arrangement of fibers Empirical model C_1 and C_2 depend on fiber orientation Experimentally $C_1 = 0.64$ and $C_2 = 6.1$	(C. Y. Chen, 1955)
$F = \frac{8\pi}{\left[-\ln\alpha_f - \left(\frac{1 - \alpha_f^2}{1 + \alpha_f^2}\right)\right]}$	Flow is perpendicular to fibers	(Happel, 1959)
$F = \frac{8\pi}{\left[-\ln\alpha_f + 2\alpha_f - \frac{1}{2}\alpha_f^2 - \frac{3}{2}\right]}$	Flow is perpendicular to fibers	(Kuwabara, 1959)
$F = \frac{8\pi}{\left[-\ln\alpha_f - \frac{3}{2}\right]}$	Flow is perpendicular to fibers	(Fuchs & Stechkina, 1963)
$F = \frac{4}{\pi \left[H_{Ku} + 1.996Kn_f \left(-\frac{1}{2}\ln\alpha_f - \frac{1}{4} + \alpha_f^2 \right) \right]}$	Flow is perpendicular to fibers	(Pich, 1966)
$\frac{1}{4\alpha_f^2} = \frac{1}{3\alpha_f} + \frac{5}{6\alpha_f} F^{-\frac{1}{2}} \frac{K_1}{K_0}$	Random arrangement of fibers Theoretical model $\alpha_f < 0.75$ K_0 and K_1 Bessel's functions modified by the order of 0 and 1 respectively	(Spielman & Goren, 1968)
$F = 2.446 + 38.16\alpha_f + 138.9\alpha_f^2$	Random arrangement of fibers Theoretical model	(Henry & Ariman, 1983)
$F = \frac{20}{3 \left[-\ln\alpha_f - 0.931 + (\ln\alpha_f)^{-1} \right]}$	Random arrangement of fibers Theoretical model $\alpha_f < 0.25$	(Jackson & James, 1986)

2.3.1. Pressure drop of clogged flat fibrous media

A few attempts have been made to derive a mathematical prediction of pressure drop during clogging (Bergman et al., 1978; C. N. Davies, 1973; Juda & Chrosciel, 1970; Kanaoka & Hiragi, 1990; Payatakes & Okuyama, 1982). Novick's approach (Novick et al., 1991) is quite different from the others: they considered the presence of a cake as a result of particle deposition on fiber surface. Davies' model is based on the expression he had established for a clean medium. In considering the collected mass, therefore, he assumed that particles were uniformly deposited on each fiber, increasing both the fiber diameter and medium's packing density. The major advantage of this model is that all parameters can be easily measured. Nevertheless, the impact of particle size is not considered.

In Bergman's model (Bergman et al., 1978), two types of fibers collaborate to collect particles inside the medium; first, the initial clean fibers, and second, the deposited particles, which form dendrites that act as new fibers. (Letourneau et al., 1993) demonstrated that collected particles are not distributed uniformly over the whole thickness of a medium. Surface layers are assumed to be more loaded than depth layers.

The same authors subsequently compared their experimental results with those of the Bergman model (Bergman et al., 1978), for the Most Penetrating Particle Size (MPPS) (0.15 and 0.25 μm), and reported that the Bergman model underestimates the pressure drop. They therefore proposed that in order to model pressure drop in fibrous media as a function of the deposited particle mass, the penetration profile of particles inside the fibrous media must be known. All the other models are difficult to use and validate through experiments. (Kanaoka & Hiragi, 1990), (Payatakes & Gradoń, 1980), and (Payatakes & Okuyama, 1982) have individually developed models based on determining the complex drag force acting on the fiber surface.

Novick's model (Novick et al., 1991) of fibrous media cake formation requires knowledge of the particle deposition packing density, defined as cake packing density (α_{pc}), which is difficult to derive. They assumed the pressure drop caused by the clogged media as the additional pressure drop in the clean media (Δp_0) and in the cake during particle deposition. Based on limited experimental studies, a range of values is given for α_{pc} : (A. Kirsch & Lahtin, 1975) gave values of 0.08 to 0.15 for particles smaller than $1\mu\text{m}$, while (Schmidt & Löffler, 1991) reported 0.11 and 0.21 for $3.8\mu\text{m}$ particles.

(Thomas et al., 2001) developed a new model based on observation of the clogged fibrous media scanning electron microscopy. They suggested that all collected particles form dendrites which can be assumed to act as new fibers and contribute to the increase in collection efficiency.

In this model, the medium is divided into several slices containing both types of particle collectors: medium fibers and deposited particles. Slices are defined by their thickness L_J . During filtration, slice J is considered to be homogeneously loaded with particles, and the packing density of the collected particles, $\alpha_{pJ,t}$ as a function of filtration time is given as:

$$\alpha_{pJ,t} = \frac{\text{Volume of collected particles in slice } J}{\text{Volume of slice } J} \quad (2-21)$$

The fractional air flow rate across the fibrous medium is considered to be equal to $1 - \frac{\alpha_p}{(1-\alpha_f)}$ while the rate across the dendrites is given as $\frac{\alpha_p}{(1-\alpha_f)}$.

Several correlations are used to estimate the pressure drop in fibrous media during clogging. Different models of pressure drop for clogged flat fibrous media are given in Table 2-8.

Table 2-8: Models of pressure drop for clogged flat fibrous media

Expression of Δp	Remarks	Ref.
$\Delta p = \Delta p_0 \frac{\ln \alpha_f + 2C_1}{C_2^2 (\ln(\alpha_f + \alpha_p) + 2C_1)}$	<ul style="list-style-type: none"> • Particles collect inside the medium (depth filtration) • Particles are not distributed uniformly across the fiber • C_1 and C_2 are constant 	(Juda & Chrosciel, 1970)
$\Delta p = \frac{64\mu U_0 L (\alpha_f + \alpha_p)^{\frac{3}{2}}}{\left(1 + \frac{\alpha_p}{\alpha_f}\right) d_f^2}$	<ul style="list-style-type: none"> • Particles collect inside the medium (depth filtration) • Homogeneous distribution of particles throughout the medium • Does not take into account the size of collected particles 	(C. N. Davies, 1973)
$\Delta p = 64\mu U_0 L \left(\frac{\alpha_f}{d_f^2} + \frac{\alpha_p}{d_p^2}\right)^{1/2} \left(\frac{\alpha_f}{d_f} + \frac{\alpha_p}{d_p}\right)$	<ul style="list-style-type: none"> • Particles collect inside the medium (depth filtration) • Homogeneous deposition of particles throughout the medium • Uniformity in particle diameter throughout the medium • Takes into consideration the mean size of collected particles • Two types of fibers considered: clean fibres, and dendrites formed by deposited particles 	(Bergman et al., 1978)
$\Delta p = \frac{64\mu U_0 \alpha_f^{\frac{1}{2}}}{k d_f} \left(\frac{2\alpha_f d_p}{3d_f^2} \left[(1 + \beta)^{\frac{3}{2}} - (1 + \beta \exp^{-kL})^{\frac{3}{2}} \right] + 2 \frac{\alpha_f}{d_f} \left[(1 + \beta)^{\frac{1}{2}} - (1 + \beta \exp^{-kL})^{\frac{1}{2}} \right] + \frac{\alpha_f}{d_f} \ln \frac{\left[(1 + \beta)^{\frac{1}{2}} - 1 \right] \left[(1 + \beta \exp^{-kL})^{\frac{3}{2}} + 1 \right]}{\left[(1 + \beta)^{\frac{1}{2}} + 1 \right] \left[(1 + \beta \exp^{-kL})^{\frac{3}{2}} - 1 \right]} \right)$ $\beta = \frac{k}{\rho_p \alpha_f (1 - \exp^{-kL})} \left(\frac{d_f}{d_p}\right)^2 \frac{m}{\Omega}$	<ul style="list-style-type: none"> • Particles collect inside the medium (depth filtration) • k is the medium penetration factor • $\frac{m}{\Omega}$ is the area density of collected particles • Does not take into account the homogeneous deposition of particles throughout the medium • Satisfactorily translates the evolution of pressure drop across a high-efficiency medium when it undergoes deep clogging • Strongly dependent on the penetration factor • Does not take into account the variation in penetration factor during clogging or the variation in mean diameter of collected particles based on the thickness of the medium • Mean diameter of collected particles is constant and equal to the mean diameter of aerosol particles 	(Letourneau et al., 1991)

$\Delta p = \Delta p_0 \int_0^L \frac{C_{Tm}(l,t)}{C_T} \frac{d_{fm}(l,t)}{d_f} \frac{dl}{L}$ $V_c = \frac{4m_{LF}}{\pi\rho_p d_f^2}$ $\frac{d_{fm}(l,t)}{d_f} = 1 + aV_c \quad \text{If } V_c < 0.05$ $\frac{d_{fm}(l,t)}{d_f} \propto \sqrt{bV_c + c} \quad \text{If } V_c > 0.05$	<ul style="list-style-type: none"> • Particles collect inside the medium (depth filtration) • Particles do not accumulate homogeneously on the fibers • Agreement between the model and the experiment on real fibrous media is less satisfactory • This model can only be applied if the equations relating the fiber diameter and drag coefficients to the mass of collected particles are known • C_T and $C_{Tm}(l,t)$ are the drag coefficients for virgin fibers and loaded fibers, respectively, and $d_{fm}(l,t)$ is the diameter of the loaded fiber • V_c is the dimensionless volume of collected particles • m_{LF} is the mass of collected particles per unit length of fiber • a, b and c are experimental constants 	<p>(Kanaoka & Hiragi, 1990)</p>
$\Delta p = \frac{h_k a_g^2 \alpha_{pc} \mu}{[C_c (1 - \alpha_{pc})^3 \rho_p]} U \frac{m}{\Omega}$	<ul style="list-style-type: none"> • Particles form a cake (surface filtration) • Pressure drop due to the medium (Davies' law) and the cake (Kozeny-Carman relationship) • Packing density assumed constant over cake thickness • There is no compression on the cake • a_g is the particle specific area • h_k is the Kozeny constant • $h_k = 5$ for spherical particles 	<p>(Novick et al., 1991)</p>

$\Delta p_{J,t} = 16\mu U_0 L_J \left(\frac{4\alpha_f}{d_f^2} + \frac{4\alpha_{pJ,t}}{\bar{d}_{pJ,t}^2} \right)^{1/2} \left(\frac{2\alpha_f}{d_f} + \frac{2\alpha_{pJ,t}}{\bar{d}_{pJ,t}} \right) \left[1 + 56(\alpha_{pJ,t} + \alpha_f)^3 \right]$ $\Delta p = \sum_{J=0}^{n_p} \Delta p_{J,t}$	<ul style="list-style-type: none"> • Particles collect inside the medium (depth filtration) and on its surface (surface filtration) • Medium divided into several slices • Bergman's model used for depth filtration • Novick's model used for surface filtration • Dendrite considered to be a fiber • Particle penetration profile is considered • Overestimates the pressure drop during depth filtration • Underestimates the accumulated mass at clogging point • $\Delta p_{J,t}$ is the pressure drop in each slice 	<p>(Thomas et al., 2001)</p>
$\Delta p = 18 \frac{\mu U}{\rho_p C_c} \frac{v(\alpha_{pc})}{(1 - \alpha_{pc})^2} \frac{\kappa}{d_{vg}^2 \exp(4 \ln^2 \sigma_g)} \frac{m}{\Omega}$	<ul style="list-style-type: none"> • Particles form a cake (surface filtration) • Novick's model modified for non-spherical particles • Widely used to determine the pressure drop of a nanostructure deposit in the Stokes regime • Pressure drop is the sum of the drag forces acting on all particles forming the cake • $v(\alpha_{pc})$ is the void function which makes it possible to consider the effect of neighbouring particles • Applicable to soot agglomerate deposits • $\kappa = 1$ which is the dynamic shape factor of the particles • Size distribution of the spherical primary particles is considered • Size distribution of the agglomerates is not considered • Partial overlapping of particles making up the cake is not considered 	<p>(Endo et al., 2002)</p>

$\Delta p = \frac{64\pi\alpha_{pc}^{1/2}(1 + 56\alpha_{pc}^3)}{C_c d_p^2 \rho_p} \frac{(1 - Co)}{\left[\frac{2}{3} - Co^2\left(1 - \frac{Co}{3}\right)\right]} \mu U \frac{m}{\Omega}$	<ul style="list-style-type: none"> • Particles form a cake (surface filtration) • Based on Davies' law for a nanoparticle cake • Nanostructure deposit assumed to be a tangle of chains composed of juxtaposed particles with (aggregates) or without (agglomerates) partial overlapping • Uses the drag force acting on the particle chain rather on particles • Cake packing density is determined by agglomerate or aggregate diameters whereas pressure drop is linked to particle primary diameter and overlap coefficient • Co is the overlap parameter which is equal to: $Co = \frac{(d_p - d)}{d_p}$ where d is the distance between two particles in contact if $Co = 0$ the primary particles are in point contact (juxtaposed particles) if $Co = 1$ the particles are completely merged • d_p is the diameter of average mass which is equal to: $d_p = d_{pG} \exp[1.5 \ln^2(\sigma_g)]$ • $\alpha_{pc} = 1 - \frac{1+0.44Pe}{1.019+0.46Pe}$ $Pe = \frac{U d_{agg}}{D}$ 	<p>(Thomas et al., 2014)</p>
$\Delta p = \frac{32U_p \mu L^*}{d_{eq}^2}$ <p>(Capillary approach for depth filtration)</p> $L^* = \alpha_f L$ $U_p = \frac{U}{1 - \alpha_f}$	<ul style="list-style-type: none"> • Particles collect inside the media (depth filtration) and on its surface (surface filtration) • Capillary approach used for depth filtration • Thomas' model (2014) used for surface filtration 	<p>(Bourrous et al., 2016)</p>

These models can be classified into two main groups: capillary models and particulate models. The most prominent correlation based on a capillary model is the Kozeny-Carman equation in Stokes regime. In this approach, the porous medium is considered to be an assembly of capillaries of particular size and geometry through which fluid flows. There are many relationships for determining Kozeny's constant, all of which are a function of the packing density of the deposited particles. Table 2-9 lists some of the expressions found in the literature. Particulate models are based on flow around particles. (Mauret & Renaud, 1997) and (Punčochář & Drahoš, 2000) have determined the applicability range of these models. In the case of fibers, (Mauret & Renaud, 1997) demonstrated that the capillary approach is less appropriate for packing densities greater than 0.75 ($\alpha_f > 0.75$) and for Reynolds numbers below 100 ($Re < 100$). Since the packing density of nanostructured deposits is very high, ranging from 90% to 98% (Andersen et al., 2002; S. C. Kim et al., 2009; J. Liu et al., 2013), the approach based on capillary models is not relevant.

Table 2-9: Kozeny's constant relationships

Expression	Range of validity	Ref.
$h_k = 5.55$	$0.2 < \alpha_{pc} < 0.6$	(Fowler & Hertel, 1940)
$h_k = 4 \frac{(1 - \alpha_{pc})^3}{\alpha_{pc}^{1/2}} (1 + 56\alpha_{pc}^3)$	$0.006 < \alpha_{pc} < 0.3$	(C. N. Davies, 1973)
$h_k = 4.7 + e^{14(0.2 - \alpha_{pc})}$	$0.01 < \alpha_{pc} < 0.4$	(F. Chen, 1975)
$h_k = 5 + e^{14(0.2 - \alpha_{pc})}$	$0.04 < \alpha_{pc} < 0.42$	(F. Chen, 1975)
$h_k = 3.5 \frac{(1 - \alpha_{pc})^3}{\alpha_{pc}^{1/2}} (1 + 57\alpha_{pc}^3)$	$0.01 < \alpha_{pc} < 0.6$	(Ingmanson & Andrews, 1963)

2.4. Estimating the packing density of the deposited particles (α_{pc})

Packing density is a significant parameter for the estimation of pressure drop during dynamic performance of the medium. It can be determined using direct or indirect measurements. An example of the former is to measure the thickness and mass of the deposit; thickness can be measured by observing a slice of the medium by means of a cathetometer, an optical microscope, SEM or interferometry (Callé, 2000; Joubert, 2009; Penicot Baugé, 1998; Schmidt & Löffler, 1991), or by using laser triangulation during the filtration process (Bourrous, 2014). The mass of the collected particles is equal to the difference in mass between the clogged medium and the clean medium. If the medium is heavily clogged or if the particles are not very penetrating, this mass may be compared to the mass of the collected particles (m) on the medium area (Ω). Thus, the packing density of the deposited particles (cake) is:

$$\alpha_{pc} = \frac{m}{\Omega \rho_p L} \quad (2-22)$$

This approach can be used to obtain a packing density value for the deposit, provided it is a homogeneous deposit. However, the obtained value is strongly dependent on the percentage of uncertainty in measuring the thickness of the deposit. As (Schmidt & Löffler, 1991) have proposed in regard to solving the uncertainty issue, dealing with greater thicknesses will lead to minimization of the uncertainty related to thickness values.

Indirect measurement, based on modeling of the linear evolution of the pressure drop, will use a model and adjust its packing density values. The obtained packing density cannot be separated from the related pressure drop expression and does not, in any case, define the real value of the packing density of the cake. This method was used by (Penicot Baugé, 1998) with the Kozeny-Carman model, validated across a range of packing densities from 0.2 to 0.7. Applying this method

to experimental data on pressure drop evolution demonstrates a relationship between calculated packing density and the mass median diameter of the particles that form the deposit.

As a result, the packing density of the cake is as follows:

$$\alpha_{pc} = 0.58 \left[1 - \exp\left(\frac{-d_p}{0.53}\right) \right] \quad (2-23)$$

This evolution is confirmed by (Brock & Tarleton, 1998) simulation of the formation of a particle deposit and also by the simulation by (Jeon & Jung, 2004). They demonstrated that a low adhesive force between the particles leads to a denser particle structure. (Kasper et al., 2010) propose the following relationship based on their observation of monodisperse spherical polystyrene particles deposited on steel fibers with a diameter of 8 and 30 μm :

$$\alpha_{pc} = 0.64[1 - \exp(-290\rho_p d_p)] \quad (2-24)$$

(Yu et al., 2003) propose an empirical relationship (Eq. 2-25) based on tests they performed on aluminum oxide powders with a median diameter ranging from 2.8 to 54 μm (Yu et al., 1997).

$$\alpha_{pc} = 0.606[1 - \exp(-275d_p^{0.468})] \quad (2-25)$$

2.5. Parameters affecting nanoparticle filtration efficiency

2.5.1. Effect of face velocity and air flow rate

The face velocity or airflow rate can considerably affect the overall filtration efficiency of fibrous media (Alonso et al., 1997; Bahloul et al., 2014; Kousaka et al., 1990; Mostofi et al., 2010). At low face velocity, diffusion and electrostatic forces collaborate considerably to capture particles due to higher residence time. As face velocity increases, the interception mechanism becomes dominant while the diffusion mechanism contributes much less to the medium's filtration efficiency. Therefore, it is expected that filtration efficiency will drop significantly at higher face velocities. (Boskovic et al., 2007; Boskovic et al., 2008) conducted experiments at velocities

ranging between 5 and 20 cm/s for different shapes of particles. Generated particles were in the range of 50 to 300 nm. The results demonstrated that at lower face velocities the filtration efficiency of fibrous media increased for all particle shapes. (Balazy et al., 2004) studied filtration efficiency and pressure drop at air velocities in the range of 10 to 30 cm/s for particle sizes between 10 and 500nm. The results showed that filtration efficiency decreased when air velocity increased. (S. C. Kim et al., 2007a) carried out an experiment with face velocities in the range of 5.3, 10, and 15 cm/s using silver nanoparticles between 3 and 20 nm. The results demonstrated that with an increase in face velocity, filtration efficiency decreases due to shorter residence time in the fibrous medium.

2.5.2. Effect of humidity

Humidity is one of the factors that may have an effect on the filtration efficiency of fibrous media (Mahdavi et al., 2015; Mostofi et al., 2010). Due to lack of studies, the effects of humidity are not well understood. In general, high relative humidity decreases the flow resistance of fibrous media when loading with hygroscopic particles, but has no influence in the case of non-hygroscopic particles (Gupta et al., 1993; Joubert et al., 2010; Miguel, 2003). (Joubert et al., 2011) carried out an experiment with varying levels of humidity and demonstrated that, with higher relative humidity in the range of 20 to 60%, specific cake resistance is decreased and does not rely on the mass of the loading particles.

The properties of hygroscopic particles are influenced by particle size and have been demonstrated to occur below the relative humidity condition at deliquescence point for nanometer-sized particles (Biskos et al., 2006). For low relative humidity ($RH < 70\%$) and nanometer-sized particles ($d_p < 200$ nm), the growth factor (i.e., the change in particle size from the diameter in dry conditions, which depends on particle size) is larger for smaller particles and higher relative humidity (Hu et

al., 2010). NaCl has also been demonstrated to have a reversible uptake of liquid water on the surface for relative humidity below deliquescence point, which can have an effect on particle shape and structure (Wise et al., 2008). The work of (Hu et al., 2010), demonstrates that hygroscopic particles exhibit a GF between 0 and 10% for particles in the range of 20 to 200 nm over a relative humidity between 0 and 70%. Physical changes in particle structures formed on the fiber surface are responsible for alterations in the properties of loaded media under relative humidity conditions. A recent investigation by (Montgomery et al., 2015) showed the impact of relative humidity on the properties of air fibrous media loaded with hygroscopic and non-hygroscopic particles. NaCl and Al₂O₃ particles were loaded on commercial fibrous media in a laboratory. After testing at the desired relative humidity, they were exposed to clean air. Consequently, both flow resistance and filtration efficiency decreased. The changes were found to be irreversible in nature, showing an underlying physical change in the structure of the captured dust. No changes were seen for the clean medium or for fibrous media with adhering non-hygroscopic particles.

The authors of that study presented an explanation for the physical change in particle properties underlying the change in medium characteristics. They posited that the loaded particles on the fiber could have changed in size when exposed to a high level of relative humidity. This increase in particle size could exert stress on the structure of captured dust.

To confirm this hypothesis, the changes in particle aggregate structure with relative humidity need to be identified and quantified through further research.

(C. S. Kim et al., 2006) subjected particles smaller than 100nm to three humidity conditions of 10.6, 305 and over 23000 ppm corresponding to 0.04, 1.22 and 92% relative humidity respectively, and did not find any observable effects on filtration efficiency. However, (Hinds, 1999; Miguel, 2003) demonstrated that for coarse particles, filtration efficiency increased with relative humidity.

(C. S. Kim et al., 2006) posited that an increase of the capillary force at higher relative humidity would increase the adherence between fibers and particles. However, the attraction between particles and fibers due to capillary force is only significant for larger particles.

Studies on electret fibrous media have shown that filtration efficiency decreases as humidity increases. The reason is that higher relative humidity eliminates the charges on both fibers and particles (Mostofi et al., 2010). (Ikezaki et al., 1995) and (Łowkis & Motyl, 2001) demonstrated that the potential of electret fibrous media for collecting nanoparticles falls as the surface charge is decreased under higher relative humidity. (Yang & Lee, 2005) however, showed that relative humidity has no impact on particle penetration through the electret fibrous medium for monodisperse NaCl particles between 50 and 100 nm. In addition, they argued that other investigations charged the electret fibrous media mainly through corona or triboelectric charging methods, which makes the ions and electrons on the fibers readily removable by the water molecules. In their investigation, Yang & Lee charged the media by coating them with negative carbon chain-group ions, which makes the surface charge less affected by relative humidity.

2.5.3. Effect of particles shape and morphology

Particle shape has been shown to affect filtration efficiency for nanoparticles in fibrous media. (Boskovic et al., 2005) performed an experiment with polystyrene latex (PSL) spheres, spherical particles of iron oxide, and perfect cubes of magnesium oxide. The polypropylene medium used in this experiment was 2mm thick and had a packing density of 0.09. The fiber diameter was 19 μm and the face velocity was 0.02 m/s. The results demonstrated that, for particle sizes between 50 and 300 nm, the filtration efficiency was much lower for cubic particles than for spherical particles of the same electrical mobility diameter, and it improved as the particle size increased. The explanation given by Boskovic is that particles of different shapes move differently on the fiber

surface. Spherical particles slide or roll before coming to rest, while cubic particles slide or tumble. Tumbling can considerably change the contact area between particle and fiber surface, thereby increasing the possibility of the particle detaching from the fiber. Note that detachment due to tumbling differs from thermal rebound.

In a subsequent investigation (Boskovic et al., 2007), a 3mm-thick polypropylene medium was soaked with mineral oil and then squeezed to remove excess oil. The medium had a packing density of 0.184 and the fiber had a mean diameter of $12.9\mu\text{m}$ with a standard deviation of 1.4. Using spherical PSL particles and cubic MgO particles between 50 and 300 nm in electrical mobility diameter, filtration efficiencies were determined for two face velocities, 0.1 and 0.2 m/s. No significant difference in filtration efficiency was observed between spherical and cubic particles of the same electrical mobility diameter. The results showed that absorption of the particles' kinetic energy by the oil film had effectively restrained particle motion on the fiber after collision and thereby decreased the probability of detachment. This supports the hypothesis that the type of particle motion on the fiber surface after collision can have an effect on filtration efficiency.

(Boskovic et al., 2008) also carried out another series of experiments with spherical PSL particles, perfect cubes of MgO particles, and cubic NaCl particles with rounded corners. The 2mm-thick polypropylene medium had a packing density of 0.29 and a fiber diameter of $12\mu\text{m}$. The experiments were conducted with three face velocities, 0.05, 0.1 and 0.2 m/s. The results demonstrated that, when inertial effects were inconsequential at $U_0 = 0.05$ and 0.1 m/s, the filtration efficiencies for 100nm particles were in the following order: PSL particles > NaCl particles > MgO particles. The order can be explained by the fact that a cubic NaCl particle with rounded corners will tumble if it hits a fiber with one of its sharp edges, but will roll if it hits with one of its rounded corners. As a result, the intermediate-shaped NaCl particle has a detachment

probability that lies between that of a sphere and that of a perfect cube. At $U_0 = 0.2$ m/s, there is no significant difference in filtration efficiency between cubic MgO particles and intermediate-shaped NaCl particles, because the improvement due to inertial impaction for the denser (heavier) MgO particles sufficiently offsets the higher probability of detachment.

2.5.4. Effect of fiber diameter

The medium is assumed to be constituted by uniform fibers. From the equation of single fiber efficiency, it can be seen clearly that the single fiber efficiency due to interception of diffused particles is higher for finer fibers. Also, filtration efficiency increases as fiber diameter decreases. As a result, media composed of finer fibers have a better filtration efficiency for nanoparticles.

(Hinds, 1999) measured filtration efficiency as a function of particle size for three fibrous media having the same pressure drop, packing density (0.05), and face velocity (0.1 m/s), with fiber diameters of 0.5, 2, and 10 μm . The results demonstrated that the medium with the finest fibers yielded the smallest MPPS and the highest minimum efficiency. It also gave a higher quality factor, but only for particles larger than 0.2 μm .

The quality factor, which is used to measure performance, is determined mainly by particle collection efficiency and pressure drop. The best medium has the highest filtration efficiency and lowest pressure drop. The quality factor is given as (Hinds, 1999):

$$Q_F = \frac{-\ln(1-\eta)}{\Delta p} \quad (2-26)$$

The term nanofiber has been used to characterize fibers smaller than 1 μm in diameter. (Podgórski et al., 2006) conducted an experiment using one conventional microfiber medium and five dual-layer media composed of a poly-disperse nanofiber layer and a poly-disperse microfiber support layer. The particles collected were poly-disperse liquid DEHS particles ranging in size from 10 to

500 nm, at a face velocity of 0.0894 m/s. The nanofibers had mean diameters in the range of 0.74 to 1.41 μm ; the media were between 1.4 and 5.5 mm thick, with packing densities in the range of 0.014 to 0.035. The microfibers had a mean diameter of 18 μm ; the medium was 2.1 mm thick, with a packing density of 0.149. The results demonstrated that the filtration efficiency of all five dual-layer media was considerably higher than that of the microfiber medium tested alone, for particles in the MPPS range. Because the elevation in pressure drop due to the addition of a nanofiber layer was moderate, four of the five dual-layer media had quality factors higher than that of the microfiber medium. Only one dual-layer medium had a lower quality factor for particles smaller than 30 nm.

Yun (Yun et al., 2007) employed poly-acrylonitrile nanofiber to investigate filtration of monodisperse NaCl particles in the range of 10 to 80 nm at a face velocity of 0.053 m/s. The nanofibers, 0.27 μm in diameter, were produced using the electrostatic spinning process. The five nanofiber media had thicknesses between 0.004 and 0.02 mm and packing densities in the range of 0.112 to 0.152. The results demonstrated that, to have the same level of filtration efficiency as commercial fibrous media, the nanofiber media required a considerably lower mass but a higher pressure drop. For a given particle size, the filter quality factor and single fiber efficiency for nanofiber media relied on packing density and fiber diameter.

(J. Wang et al., 2008) carried out an investigation using four media, each constituted of a layer of nanofibers placed on a substrate made of micrometer fibers. The nanofiber diameter was 0.15 μm , the effective packing density was between 0.034 and 0.134, the face velocity was 0.10 m/s, and the particle diameter was between 3 and 780 nm. It was observed that both filtration efficiency and pressure drop increased as the packing density of the nanofiber layer rose. Because of the considerable increase in pressure drop, the addition of nanofibers was only capable of improving

the quality factor for particles larger than about 100 nm. Wang also established a numerical model for nanofiber media. The simulation results were in good agreement with the experimental data for particles larger than 20 nm.

In a more recent study with three sizes of electro-spun Nylon 6 nanofibers (94, 185 and 220 nm in diameter), (Hung & Leung, 2011) demonstrated that the finer nanofiber media gave higher filtration efficiencies for particles between 50 and 200 nm than did the coarser media, mainly because of greater diffusion and interception. However, the pressure drop was considerably higher for the finer media.

For filtration of particles in the range of 50 to 90 nm, the 185 nm-fiber medium had a better quality factor than the 94 nm-fiber medium, but the opposite was true for particles between 100 and 380 nm.

It has been demonstrated that growing multi-walled carbon nanotube (MWCNT) fibers on a fibrous medium can increase nanoparticle filtration efficiency without a noticeable increase in pressure drop.

2.5.5. Effect of heterogeneous fibers

Fibrous structure is complicated and difficult to model (Brown, 1993; C. N. Davies, 1973). Most investigators tend to simplify the medium as an array of uniform fibers. Heterogeneities in structure have a significant effect on fibrous medium efficiency (A. Kirsch & Stechkina, 1973; A. Kirsch et al., 1974).

There are two main kinds of medium heterogeneity. In one of them the medium consists of fibers not uniformly distributed over the medium (Adam et al., 1992; Dhaniyala & Liu, 2001a; Dhaniyala & Liu, 2001b; Heidenreich et al., 1991; Molter & Fissan, 1997). In the other, the fibers have a

wide range of diameters uniformly distributed over the medium (Bao et al., 1998; Podgórski et al., 2006; Sakano et al., 2000).

Steffens & Coury, (2007) proposed considering the medium as a superimposition of n fibrous media, each one consisting of fibers with a narrower size range (A. Kirsch & Stechkina, 1973; Sakano et al., 2000). Consequently, the whole medium can be simplified as a sequence of n media of height L and packing density α_i , each consisting of fibers with diameter d_{fi} . The packing density α_i can be readily correlated to the medium's overall packing density α , by the following relation:

$$\alpha_{fi} = 1 - (\alpha_f \times x_i) \quad (2-27)$$

Where x_i is the number fraction of fibers with diameter d_{fi} , given by:

$$x_i = \frac{n_i d_{fi}}{\sum n_i d_{fi}} \quad (2-28)$$

Where n_i is the number of fibers with a given diameter d_{fi} .

Therefore, the total efficiency is given as:

$$\eta = 1 - \exp \left[\frac{-4L}{\pi} \sum_{i=1}^n \frac{\alpha_f}{(1-\alpha_{fi}) d_{fi}} \frac{\pi}{d_{fi}} \right] \quad (2-29)$$

Steffen and Coury (Steffens & Coury, 2007) conducted an experiment to validate the model for a HEPA filter with heterogeneous fibers. The medium had a packing density of 0.08, a thickness of 0.4 mm, and a fiber median diameter of $0.45 \mu\text{m}$. Mono-dispersed nanoparticles between 8.5 and 94.8 nm were chosen, with face velocities of 0.03 to 0.25 m/s. The results demonstrated that the predictions underestimate the results. It was suggested that the existing correlation be corrected by characterizing the medium as constituted of several media in series, each with a fiber diameter and packing density obtained from the fiber size distribution.

2.5.6. Effect of electrostatic forces

Application of electrostatic forces can considerably enhance filtration efficiency. The process of aerosol filtration in the presence of electrostatic forces is complex. Past investigations have led to a good understanding of the filtration process in clean fibrous media, but there is a notable gap between theory and experiment when it comes to the impact of electrostatic forces on filter efficiency (C. Wang, 2001).

The electrostatic effect is generally useful for improving the collection of particles ranging in size from 0.15 to 0.5 μm , which are difficult to capture by other mechanisms. Filtration efficiency in the presence of electrostatic forces is affected by factors such as chemical composition of particles and fibers, charges on particles, charge density on the fiber surface, and the intensity of the externally exerted electric field (Mostofi et al., 2010).

There are generally two ways of employing electrostatic forces on both fibers and particles: one is charging the particles and the other is creating an electric field inside the medium. When the charges on the particle and the fiber are of opposite polarities, a Coulomb force is generated, whereas if the particle is charged and the fiber is neutral, or vice-versa, a polarization or image force is created. Generally, the term “polarization force” is used when the charge is on the fiber, and “image force” when the charge is on the particle. Two comprehensive reviews about the effect of electrostatic mechanisms in aerosol filtration can be found in (Brown, 1993; Shapiro et al., 1988).

Alonso (Alonso et al., 2007) investigated the impact of image force on the diffusional deposition of aerosols on wire screens. An experiment was carried out with particles carrying elementary charges of 0, +1, +2 or +3, at three different flow rates, and using two types of wire screens. The image force dimensionless number (N_{IM}) was between 10^{-7} and 10^{-5} . Two different correlations

were suggested: one which best fit the experimental data; and a second one based on the theoretical expectation that the image force deposition efficiency is proportional to the square root of the dimensionless number (N_{IM}). The experiment demonstrated that the image force effect is considerable, even for singly charged small particles. (Thomas et al., 2013) conducted an experiment using dielectric meshes and charged and uncharged copper and carbon nanoparticles in the range of 4 to 80nm. The results for the stainless-steel meshes were in good agreement with the equation for single fiber efficiency due to diffusion (Cheng & Yeh, 1980). For the polymer fiber meshes, however, the results deviated largely from this expression. Moreover, neutral aerosol penetration did not improve steadily as the particle diameter increased.

The above results reported by (Thomas et al., 2013) demonstrate that filtration efficiency due to electrostatic forces improves with particle size; for example, it can be enhanced by 20–30% when the particle diameter increases to 100nm. This effect is much more noticeable than any other investigators reported in the past (C. S. Kim et al., 2006; Yun et al., 2007). Almost all other researchers had found that nanoparticle filtration efficiency due to electrostatic forces was inconsequential.

For nanoparticles, the analytical solution of the transient charging equation has been calculated following the Fuchs theory (Fuchs, 1963). In this theory, the space surrounding a particle is divided into two regions. In the outer region, ions move based on the continuum diffusion equation, while in the inner region they move as in a vacuum, i.e., they have no collision with air molecules. (Hoppel & Frick, 1986) demonstrated that for particles smaller than 20 nm, the probability of a particle obtaining two or more net charges of either sign is practically zero. Consequently, there are only three different charges for particles smaller than 20nm: neutral, singly positive and singly negative. (Alonso et al., 2002) recalculated the ion attachment rate coefficient according to the

Fuchs theory for particle diameters in the range of 2 to 20 nm. They understood that the probability of negative ions attaching to positive particles is greater than that of positive ions attaching to negative particles. Similarly, the probability of negative ions attaching to neutral particles is greater than that of positive ions attaching to neutral particles. So, at the end of the neutralizing process, negatively charged particles are prevailing over positive ones for particles smaller than 20 nm.

On the other hand, (Hogan et al., 2009) tested positive unipolar diffusion charging between particles ranging in size from 50 to 200 nm. They demonstrated that the larger particles were able to obtain more net charges.

(Marlow & Brock, 1975) showed that there was a considerable difference in polarity between larger and smaller particles when they pass through the same bipolar charger. In the process of charging poly-disperse particles, due to unequal charging rates, large and small particles may demonstrate different polarities. Based on the above analysis, we understand that during the neutralizing process, particles smaller than 20 nm get different charges compared to the larger ones and consequently demonstrate a different level of filtration performance. Electrostatic forces might therefore have an adverse effect on filtration efficiency, in the case of small particles. On the other hand, larger particles have different charges from smaller ones, so in their case electrostatic forces actually improve filtration efficiency (Givehchi et al., 2015).

2.5.7. Effect of upstream particles concentration

In aerosol filtration theory, the effect of upstream particle concentration on filtration efficiency has not yet been studied. In the filtration process, if nanoparticles behave like gas molecules upon impact with the surface of the fibrous media, the effect of concentration also becomes important. Therefore, besides deposition mechanisms in filtration, the effect of another mechanism similar to adsorption for gas molecules has to be taken into account.

This idea originates from adsorption theory, in which gas molecules travel toward a solid's surface and are attracted to it by Van der Waals forces. This mechanism depends on the molar concentration: as the concentration increases, more and more of the surface is covered by the gas molecules. Therefore, at higher concentrations, molecules have less chance of colliding on the surface, causing reduced adsorbent efficiency.

"To borrow the adsorption theory from gas molecules for nanoparticle adsorption, the following assumptions are considered:

- For each particle size, the transport of nanoparticles onto the medium's surface depends on particle concentration, which is valid according to aerosol dynamics.
- If particles become deposited on the surface by this mechanism, they attach to the surface, and there is no rebound. " (Tan, 2014)

The Freundlich model, which is an empirical equation, accurately describes adsorption for small nanoparticles. Single fiber efficiency based on nanoparticle concentration ($E_{Concentration}$) is thus defined according to the Freundlich model as follows (Tan, 2014):

$$E_{Concentration} = KC^n \quad (2-30)$$

where K and n are constants for a specific nanoparticle and media under certain conditions. These constants are defined empirically by considering the relationship between single fiber efficiency and particle concentration.

Finally, the total single fiber efficiency for nanoparticles (E_{Σ}), taking into account the effect of particle concentration, is given by:

$$E_{\Sigma} \cong 1 - (1 - E_D)(1 - E_{Concentration}) \quad (2-31)$$

where E_D is the single fiber efficiency based on the diffusion mechanism and $E_{Concentration}$ is the single fiber efficiency based on the effect of particle concentration.

(Givehchi, 2016) conducted an experiment in order to observe the effect of upstream particle concentration on nanoparticle filtration efficiency. She used sub-4 nm tungsten oxide particles moving through different electro-spun Nano-fibrous media with the particle concentrations of $10^8, 10^7$ and $10^6/Cm^3$ with three different dilution ratios (no dilution, 1:10 and 1:100). The results demonstrated the different behaviors for nanoparticles smaller and larger than 1.96 nm during the filtration process. A noticeable drop in efficiency occurs for particles smaller than 1.96 nm. It is demonstrated that in addition to the deposition mechanisms, adsorption is also important for this range of particle sizes. Based on adsorption theory, at higher particle concentrations, particles have less chance of colliding on the medium's surface and reducing the filtration efficiency.

2.5.8. Effect of temperature

In aerosol filtration theory, the effect of temperature on nanoparticles filtration efficiency has not been studied in details. In the filtration process by increasing the temperature, the probability of rebounding nanoparticles from the surface of the fiber will increase. This is because of that, by improving the temperature, thermal speed of the particles will increase.

Previous studies on high temperature filtration have been basically focused on the micrometer size range (De Freitas et al., 2006; Hemmer et al., 2003). Therefore, it is important to study nanoparticle filtration at elevated temperatures.

The dynamic viscosity as a function of absolute temperature is derived using the Sutherland formula is given by (M. Allen & Raabe, 1982):

$$\mu_T = \mu_{23} \left(\frac{T}{T_0} \right)^{3/2} \left(\frac{T_0 + 110.4}{T + 110.4} \right) \quad (2-32)$$

where μ_{23} is the reference viscosity at 296.15 K.

The mean free path is function of temperature and pressure, which is given as (Willeke, 1976):

$$\lambda = \lambda_0 \left(\frac{T}{T_0}\right) \left(\frac{P_0}{P}\right) \left(\frac{1 + \frac{110.4}{T_0}}{1 + \frac{110.4}{T}}\right) \quad (2-33)$$

where λ_0 is the 67.3 nm for air at *STP*, T_0 is the reference temperature, which is equal to 296.15 K, P_0 is the reference pressure, which is equal to 101.35 kPa, T is the air temperature in the filter upstream inside the filter holder, and P is the air pressure inside the filter upstream inside the filter holder.

By calculating the dependency of dynamic viscosity, slip correction factor and diffusion coefficient on temperature, finally, the single fiber efficiency due to diffusion for constant face velocity is given by:

$$E_D \sim T \quad (2-34)$$

Figure 2-2 clearly demonstrates the theoretical evolution of the penetration of the system as a function of temperature (Mouret et al., 2011).

Shin et al 2008 (Shin et al., 2008), conducted an experiment to investigate the effect of elevated temperature on filtration efficiency of nanoparticles. They used a screen mesh at elevated temperatures up to 500 K for silver nanoparticles between 3 to 20 nm. A small change in the single fiber efficiency with temperature was reported for a constant flow rate as is predicted by classical filtration theory.

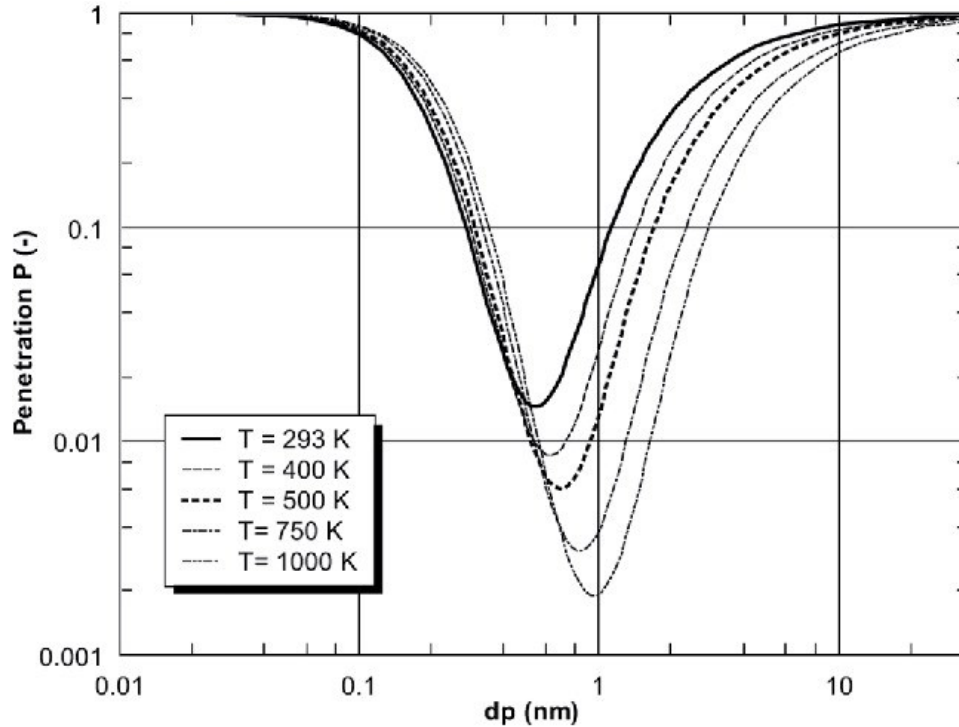


Figure 2-2: Theoretical evolution of the penetration as a function of temperature (Mouret et al., 2011)

2.6. Standards for the filter performance evaluation and the limitations

Filters used in air purification in North America are classified on the basis of their performance and stand by the U.S. standards like ANSI/ASHRAE 52.2 (American Society of Heating, Refrigerating and Air-Conditioning Engineers, 2017) (ASHRAE, 2007). This standard is limited to filter efficiency when challenged by particle size (0.3 to 10.0 μm) and then comes with a 16-point scale for minimum efficiency reporting (MERV). The higher the MERV, the more effective the filter is. Tables 2-10 and 2-11, are indicating the particle range boundaries and the MERV parameters.

**Table 2-10: Particle counters size range boundaries
(ASHRAE, 2007)**

Size range	Size range Boundaries		Geometric mean particle size (μm)
	Lower limit (μm)	upper limit (μm)	
1	0.30	0.40	0.35
2	0.40	0.55	0.47
3	0.55	0.70	0,62
4	0.70	1.00	0.84
5	1.00	1.30	1.14
6	1.30	1.60	1.44
7	1.60	2.20	1.88
8	2.20	3.00	2.57
9	3.00	4.00	3.46
10	4.00	5.50	4.69
11	5.50	7.00	6.20
12	7.00	10.00	8.37

Table 2-11: Minimum Efficiency Reporting Value (MERV) parameters (ASHRAE, 2007)

MERV	Composite Average Particle Size Efficiency (% in the size range)			Average arrestance (%)
	Range 1 0.3 to 1.0 μm	Range 2 1.0 to 3.0 μm	Range 3 3.0 to 10.0 μm	
1	--	--	$E3 < 20$	$A_{avg} < 65$
2	--	--	$E3 < 20$	$65 \leq A_{avg}$
3	--	--	$E3 < 20$	$70 \leq A_{avg}$
4	--	--	$E3 < 20$	$75 \leq A_{avg}$
5	--	--	$20 \leq E3$	--
6	--	--	$35 \leq E3$	--
7	--	--	$50 \leq E3$	--
8	--	$20 \leq E2$	$70 \leq E3$	--
9	--	$35 \leq E2$	$75 \leq E3$	--
10	--	$50 \leq E2$	$80 \leq E3$	--
11	$20 \leq E1$	$65 \leq E2$	$85 \leq E3$	--
12	$35 \leq E1$	$80 \leq E2$	$90 \leq E3$	--
13	$50 \leq E1$	$85 \leq E2$	$90 \leq E3$	--
14	$75 \leq E1$	$90 \leq E2$	$95 \leq E3$	--
15	$85 \leq E1$	$90 \leq E2$	$95 \leq E3$	--
16	$95 \leq E1$	$95 \leq E2$	$95 \leq E3$	--

According to ASHRAE, the test setup must have a square section with the dimension of 610 mm \times 610 mm. The test bench comprised of five main steps: (1) the air flow is selected; (2) the generated aerosols are injected inside the chamber, homogenized concentrations of particles are measured at upstream of the chamber; (3) the airflow passes through the filter; (4) downstream homogenized concentrations of particles are measured; and (5) finally, the airflow passes through a HEPA filter before being exhausted (Brochot et al., 2018).

2.7. Filtration of nanoparticles applied in general ventilation

In the domain of particle filtration based on the literature there are three different techniques used to evaluate the filter's performance:

- 1- Conducting an experiment on a medium and concluding these results to the filter. Generally this technique is much more appropriate for experimental studies. Although provides only the filter's "local" efficiency.
- 2- Carrying out *in situ* measurements to evaluate the filter's performance by considering the actual environment condition in which the filter is exploited. However, distinct environmental factors cannot be controlled by this technique.
- 3- Utilizing a full-scale test bench as recommended in the standards. In this method entire filters is used in the ventilation system and also is much more convenient to restrained operating conditions. Table 2-12, presents an overview of studies that have focused on the efficiency of entire filters for nanoparticles (Brochot et al., 2018).

Table 2-12: Overview of Experimental Studies on Nanoparticle Filtration Using Entire Filters
(Brochot et al., 2018)

	Filters tested		Setup(s)	Test aerosols	Velocity	Measurements	Advantages	Disadvantages
	Mechanical	Charged						
(Hanley et al., 1994)	6 filters ^(a) (25–30%, 40%, 65%, 65%, 85%, 95%)	1 filter ^(a)	Setup: Full-scale test ring (section 610 × 610 mm)	Neutralized: KCl (d_p : 0.01–3.00 μm)	Face velocity: 0.45–1.80 m/s	Size-resolved measurement: Initial efficiency + loading effects	– First paper reported with test procedure – Basis for U.S. standard	Lack of data on charged filters
(Alderman et al., 2008)	2 HEPA filters ^(b) (2 manufacturers)		Setup: Ventilation channel (section 310 × 310 mm)	Without neutralization: KCl (d_p : 70–1 000 nm)	Media velocity: 2.0–4.5 cm/s	Global measurement: Initial efficiency + loading effects	Focus on velocity effects during clogging	– Small number of filters tested – Not focused on evolution of efficiency
(Hecker & Hofacre, 2008)	24 types of filters ^(c) (MERV 6–16)		Setup: Full-scale test ring (section 610 × 610 mm)	Without neutralization: KCl (d_p : 0.03–10 μm)	Nominal fan speed	Size-resolved measurement: Initial efficiency	Empirical equation developed with curves data	Only initial efficiency measured
(Stephens & Siegel, 2013)	2 filters ^(c) (MERV 4, MERV 6)	4 filters ^(b) (MERV 10, 11, 13, 16)	In situ: HVAC system installed in unoccupied house	Without neutralization: Indoor aerosol (d_p : 0.005–0.105 μm)	Nominal fan speed	Size-resolved measurement: Initial efficiency	Representative of real environment	– Operating conditions not controlled – Only initial efficiency measured
(Shi, et al., 2013)	3 filters ^(d) (M6, F7, F8) 13 samples (8 glass fibers and 5 uncharged synthetic fibers)	5 filters ^(c) (M5, M6, F7, F8, F9) 10 samples (M5, M6, F7, F8, F9)	Setup: Full scale: According to EN 779 Small scale: Circular test section with 315 mm diameter	Neutralized: DEHS (d_p : 0.014–0.673 μm) Without neutralization: DEHS, oil aerosol, indoor aerosol (d_p : 0.014–0.673 μm)	Through filter: 0.16–0.95 m/s Through medium: 0.08–0.22 m/s	Size-resolved measurement: Initial efficiency	Global and local information on filters	– Only initial efficiency measured – No comparison between global and local efficiencies
(Karjalainen et al., 2017)	3 filters ^(d) (F7, H12, H13)	1 electret filter 1 two-stage electrostatic precipitator	Setup: Ventilation channel	Without neutralization: Aerosol generation system that mimics characteristic traffic- related aerosol (d_p : 3–200 nm)	Face velocity: 0.61–1.34 m/s	Size-resolved measurement: Initial efficiency	– Global information on filters applied to traffic- related aerosol – Study of MPPS	Only initial efficiency measured

^(a) According to ASHRAE 52-76, ^(b) according to ASME: Code on Nuclear Air and Gas Treatment, ^(c) according to ASHRAE 52.2, ^(d) according to EN 779.

Hanley et al. (1994) is the 1st printed study to measure the size-resolving efficiency of nanoparticles for entire filters. The authors observed a typical filtration efficiency curve with a higher filtration rate for smaller particles due to diffusion. They demonstrated that, the filtration efficiency increased as the particle diameter was lower than 0.1 μm and the particle diameter increased above 1 μm . As observed for media, the MPPS range is 0.1 to 1 μm for all the filters tested, whatever the filter or fiber composition is used. They also showed that efficiency decreased as face velocity increased from 0.65 to 2.25 m/s. This result was observed in the initial state of the filter and after clogging. An increase in efficiency with particle deposition was also observed. This trend was observed for all filters except the charged filter (whose medium consisted of electret fibers), which demonstrated a high initial filtration efficiency due to the electrostatic charges. Although during clogging, the efficiency of filtration decreases due to the loss of electrostatic effects. These observations are identical to those relating to filtration media.

To date, four studies have analysed size-resolved efficiency for particles smaller than 100 nm (Hecker & Hofacre, 2008; Karjalainen et al., 2017; Shi et al., 2013; Stephens & Siegel, 2013). All reported size- resolved measurements taken at the initial filtration stage only. Hecker and Hofacre (2008) tested a large number of filters for residential and commercial made by different companies. Their results correspond to the information provided by the manufacturer, although in some cases they were less efficient than manufacturer's MERV. Some of their finding are showed in Figure 2-3. The efficiency difference can be seen from MERV 6 to MERV 16. The MPPS was found in the range between 0.1 and 0.3 μm , consistent with typical filtration curves. Then they developed an empirical equation with data from these curves to predict the performance of the filter in a given MERV. Shi et al. (2013) tested in situ filters (efficiencies from F9 to M5 by European standard) and compared penetration of 0.4 μm (diameter used in European standard), for

the MPPS and for particles smaller than 100 nm. Filters were tested at different filtration rates (air velocities from 0.08 to 0.22 m/s) and three different aerosol types. The authors demonstrated that an increase in airflow rates reduced filter efficiency for particles less than 100 nm. They also showed that the MPPS was less than 0.4 μm , resulting in both neutralized and non- neutralized aerosols and for all tested filtration velocities. Hanley et al. (1994) showed the same trend in size-resolved efficiency results for entire filters and for media.

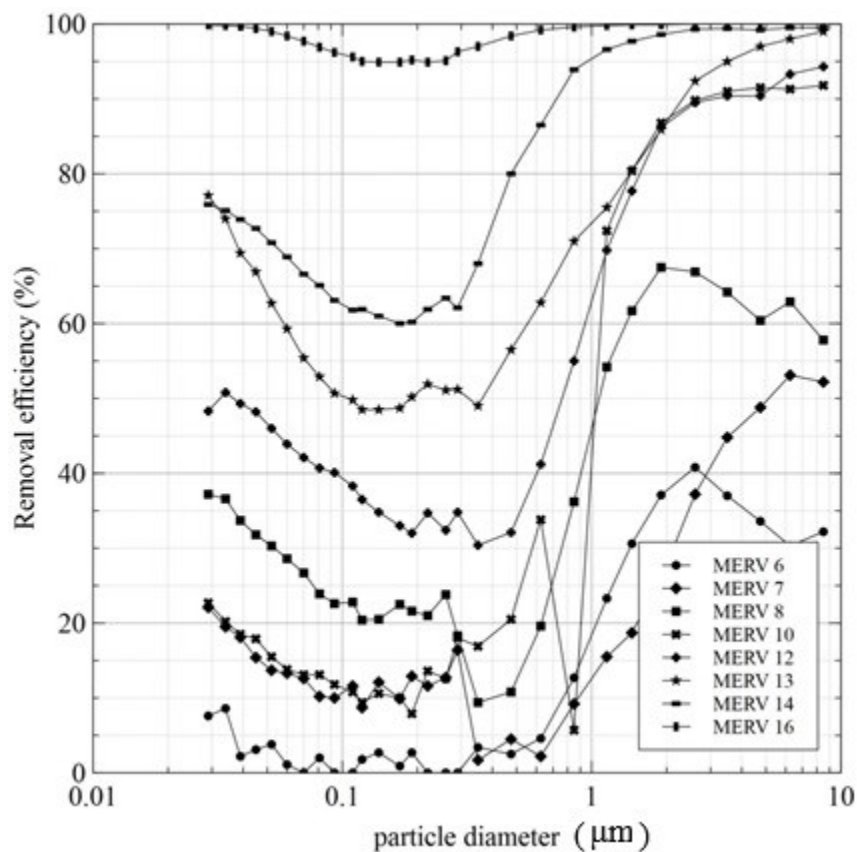


Figure 2-3: Measured collection efficiencies for 9 filters (MERV 6, 7, 8, 10, 11, 12, 13, 14, 16) (Hecker & Hofacre, 2008)

Stephens and Siegel (2013) focused on initial *in situ* filter performance for particles between 5 and 100 nm (ambient aerosol) for mechanical and electrostatic media. They measured performance when the air-handling unit normally operated with 100% air recirculation. No MPPS was observed

for mechanical filters (for particles > 100 nm), and MPPS was found to be between 20 and 30 nm for electrostatic filters. The performance of electrostatically charged filters was also not dramatically higher than that of mechanical nanoparticle filters. *In situ* measurements indicate actual filter performance. They allow all operational parameters (temperature, pressure drop and filtration velocities) to be taken into account for the filter performance. The ambient particles used in the tests also provide real filter performance information. However, *in situ* measurements have a disadvantage in that environmental parameters cannot be controlled and their precise effect on filter performance cannot be identified either in their initial state or during use. It is also very difficult to accurately identify aerosol and can change over time. This is especially important when studying electrically charged filters. Environmental parameters monitoring studies are necessary to address this problem. For example, Alderman et al. (2008) investigated the effect of face velocity on HEPA filters. Their measurements highlighted the effect of velocity on the efficiency of two different filters, although they had very low face velocities. Only global efficiency measurements were reported based on particle deposition.

Karjalainen et al. (2017) studied five commercial particle filters using a ventilation channel, with particles from 3 to 200 nm. Two generation systems (nucleation mode and soot mode) were mixed in a chamber to mimic characteristic traffic-related aerosol. Their results showed that the F7 mechanical bag- type glass filter MPPS was more than 200 nm, while the HEPA filter MPPS was about 30 nm. The MPPS values were below 50 nm for electret filters. The five articles listed in table 2-12 provide little information about filters' size-resolved efficiency based on particle parameters (charge, shape and composition), filter parameters (pleats, media) or operating conditions (temperature, humidity). Moreover, and more generally, size- resolved efficiency data are used to collect MPPS information, which is one of the main parameters of filter performance.

As discussed earlier, one of the techniques for the evaluation of particle filtration is to study the medium and extrapolate the filter results. Two studies (Chang et al., 2015; Chang et al., 2016) evaluated the five electret media penetration level in HVAC filters using neutralized nanoparticles and a medium (flat medium). Their experimental results have shown that all media have been able to capture nanoparticles. However, the penetration increased significantly as the velocity increased from 0.05 to 1 m/s, which is low in real HVAC use. They also found that penetration curves were bimodal at high velocity, with peaks at 10 to 30 nm and 150 to 200 nm respectively. Also, the first bimodal curve MPPS mode for highly charged media was higher than the second, while the reverse was true for low- charged media. These two studies show how important it is to know how the medium behaves, even if it does not provide all the keys to understanding the entire filter's behavior in the ventilation system. But no studies have been found to compare the performance of the entire filter to its medium.

Chapter 3: EXPERIMENTAL METHOD AND SYSTEM CALIBRATION

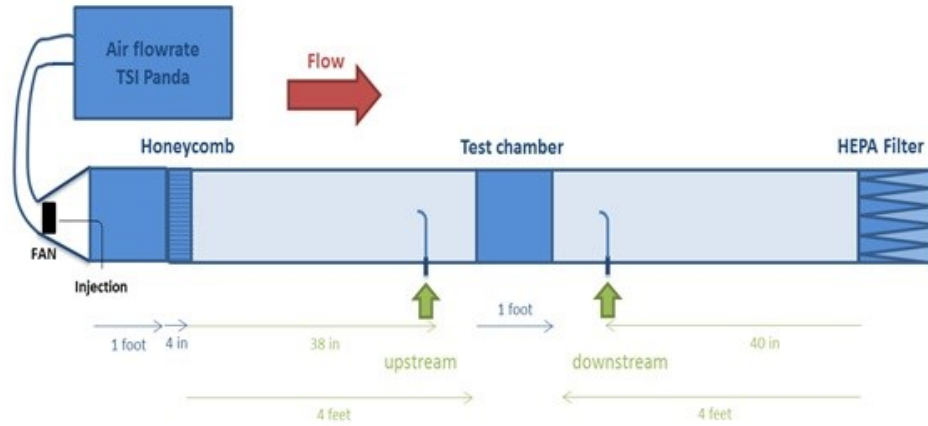
3.1. Experimental design

3.1.1. Setup configuration

Figures 3-1a and 3-1b illustrate the experimental setups used in this study. Figure 3-1a shows the small setup which has a square section of 305 mm × 305 mm (12 in×12 in). A PANDA fan from TSI regulates the flow in the setup. The NaCl particles are generated using two six-Jet Collision Nebulizers (Model CN25, BGI Inc., Waltham, MA). The particles are then injected into the test bench. A small fan and a honeycomb are installed to homogenize velocities and particles in the section. The filters are installed in the test chamber and upstream and downstream measurements will be used to measure the penetration of the filter. Penetration is thus measured for particles ranging from 22.1 to 805.8 nm using the SMPS (Scanning Mobility Particle Analyzer) for 12 in×12 in filters and at flow rates ranging from 0.25 to 1.50 m/s. At the end of the chamber, a HEPA filter is used to remove particles from the air. Figure 3-1b shows the big loop setup which has a square section of 610 mm × 610 mm (24 in×24 in). To regulate the flow a centrifugal fan was installed in the inlet of the loop. The air, filtered by a HEPA filter, is then directed to the NaCl particle generation section. The generation system consists of two collision generators: a 6-jets generator and a 24-jets generator (Model CN25, BGI Inc., Waltham, MA). Two sets of fans and the elbow of the setup allows a homogenization of the particles in the test section. The aerosols are then directed to the test section in which the filter to be tested will be installed. Then, a downstream sampling rod makes it possible to measure the concentration with or without a filter, and to give the penetration of the filter to be tested for particle sizes ranging from 22.1 to 805.8 nm using a SMPS. In this system, we are able to test 24 in×24 in filters at flow rates from 0.75 to 1.00 m/s.

The generation for both setups is provided under 30 psi pressure to generate 22.1-805.8 nm NaCl particles. The production of particles should be sufficient to measure the effectiveness of filters. NaCl particles were particularly motivated by their non-toxicity in their macroscopic form, non-explosiveness and ease of generation in Nano-metric form.

a)



b)

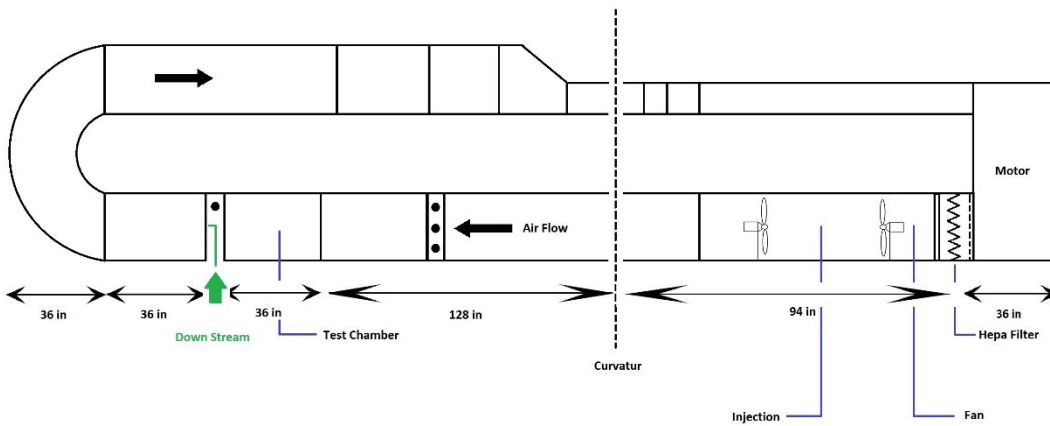


Figure 3-1: Schematic of a) the small setup; b) the big loop setup, used to challenge mechanical filters against poly-disperse NPs

3.1.2. Particle generation system

The two 6-Jet Collision Nebulizers (Model CN25, BGI Inc., Waltham, MA) are employed as an aerosol generator for the small full test system to provide poly-disperse NPs. Also for the big loop test system a 6-Jet and 24-Jet Collision Nebulizers (Model CN25, BGI Inc., Waltham, MA) are exploited as an aerosol generator (see figure 3-2). The particle generation systems for both setups were operated at an inlet pressure of 30 psi. The production of particles should be sufficient to measure the effectiveness of filters. The choice of NaCl particles was motivated in particular by its non-toxicity in its macroscopic form, its non-explosiveness and its ease of generation in Nano-metric form.



Figure 3-2: Generation system: 6-jet and 24-jet Collision Nebulizer

3.1.3. Measurement devices

A set of an “electrostatic classifier (EC)” (Model 3080, TSI Inc., Shoreview, MN, USA) with a long differential mobility analyzer (Long DMA) (Model 3081, TSI Inc.) and a “condensation particle counter (CPC)” (Model 3775, TSI Inc., Shoreview, MN, USA) is used to measure concentrations distribution for both test setups (see figure 3-3). The long DMA classified particles within a certain range of sizes based on their electric mobility diameter. The CPC then counted

classified particles. The concentration measurement technique through classification (by DMA) and counting (by CPC) is also referred as the Scanning Mobility Particle Size (SMPS). In each sample, the SMPS data for the tested size range is divided into 16 size channels. Each scan for the samples for both setups were longed with length of 137 seconds. After each scan, a 17-second retrace time was given by the device for DMA voltage adjustment.

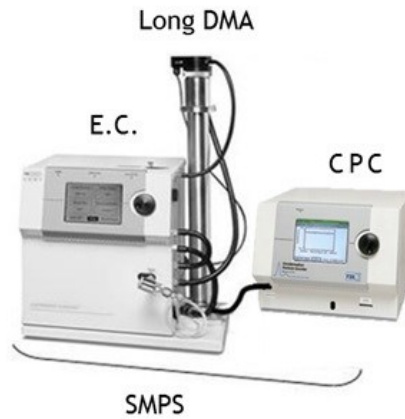


Figure 3-3: Electrostatic classifier (EC) (left) and condensation particle counter (CPC) (right)

3.2. Penetration measurement

In small setup in each test, the upstream samples are completed first, and then the sampling rod is switched to downstream. However, for big loop setup instead of changing sampling rod between upstream and downstream the tests are conducted with and without filter. For small setup each test contained 4 scans from upstream, 4 scans from downstream and again 2 scans for upstream, while, for big loop setup each test contained 4 scans without filter, 4 scans with filter and again 2 scans without filter.

In the small setup, the particle penetration through the filters is determined as the ratio of the downstream concentration (C_{down}) to upstream concentration (C_{up}) for the challenge aerosol, which is given as: (Bahloul et al., 2014):

$$P(\%) = \left(\frac{C_{down}}{C_{up}} \right) \times 100 \quad (3-1)$$

Also in the big loop setup the particle penetration through the filters is determined as the ratio of the downstream concentration of particles with filter ($C_{down-with\ filter}$) to downstream concentration of the particles without filter ($C_{down-without\ filter}$) for the challenge aerosol, which is given as follow:

$$P(\%) = \left(\frac{C_{down-with\ filter}}{C_{down-without\ filter}} \right) \times 100 \quad (3-2)$$

Therefore, the total collection efficiency (E) in both setups is defined as:

$$E(\%) = 100 - P \quad (3-3)$$

3.3. Test procedure

Figure 3-1a and 3-1b present the full schematic of the experimental setups utilized to challenge tested mechanical filter against NPs. The test systems were first set-up and calibrated according to the requirements of the ASHRAE testing standard 52.2 (2017). In the case of mechanical filters, one model of rated MERV 8 filter in three different depth sizes (1, 2 and 4in) was selected to challenge against poly-disperse NPs for both small and big loop setups. (See figure 3-4). The selected MERV 8 filter was sealed by gasket and placed in the test chambers.



Figure 3-4: Photograph of the tested filter (MERV 8) filter

One model of MERV 8 filter in three different depth sizes (1, 2 and 4in) was selected to challenge against poly-disperse NaCl aerosols for both small and big loop setups. To obtain steady state concentration in the upstream of the chambers, the generation system was allowed to work for at least 2 minutes before the penetration measurement. For each thickness three filters were used in this experiment, each penetration measurement (poly-dispersed; 22.1-805.8 nm), was repeated 2 times (N=2), for each filter and illustrated by the mean value and the standard deviation Table 3-1 summarize the experimental measurements were conducted on both setups.

Table 3-1: Summary of experimental measurements

Small Setup			
Filter	Velocity (m/s)	Thickness (in)	(Height×Width)
MERV 8	1.00, 0.75, 0.50 & 0.25	4, 2, 1	12 in×12 in 305 mm×305 mm
Big Loop Setup			
MERV 8	1.00 & 0.75	4, 2, 1	24 in×24 in 610 mm×610 mm

3.4. Setups characterization (Calibration)

Some calibration and qualification tests were conducted before the penetration test to provide reliable operating conditions for tests and sampling procedures. These calibration tests shall include:

- Measuring the velocity homogeneity at filter place, to assure the uniformity of the velocity in the test chamber.
- Conducting the stabilization test during the system start-up to determine the time interval until the particle concentration reaches a steady condition at upstream.
- Measuring the size distribution at different locations at upstream, to assure the dispersal uniformity of the challenge aerosol in the test chamber

3.4.1. Velocity homogeneity

The velocity homogeneity test was performed to assure the uniformity of the velocity at the filter place in the test chambers. To confirm this, the coefficient of variation (CV) which is defined as the ratio of standard deviation to the mean of velocity uniformity was calculated at nine upstream sampling locations (see figures 3-5 and 3-6) under three different motor flowrate (103, 203 and 324 L/s PANDA flowrate) for small setup and three different motor frequency (25, 35 and 45 Hz) for big loop setup. The measurements were inspired by the standard qualification test (ANSI/ASHRAE 52.2) with an air velocity meter VELOCICALC (TSI model 9535A). This device measures velocities in the range 0 to 30 m/s, with an accuracy of $\pm 3\%$ of reading. Each nine point were an average of one-minute measurement. The nine-point velocities were then measured in three tests. The averages of the triplicate readings at each point were then computed and the coefficient of variation of the nine points has been calculated. According to the standard, the coefficient of variation of the nine corresponding grid point air velocity values shall be less than 10% at each speed. The Figure 3-7 and 3-8 present a visualization of the velocity uniformity results in both setups.

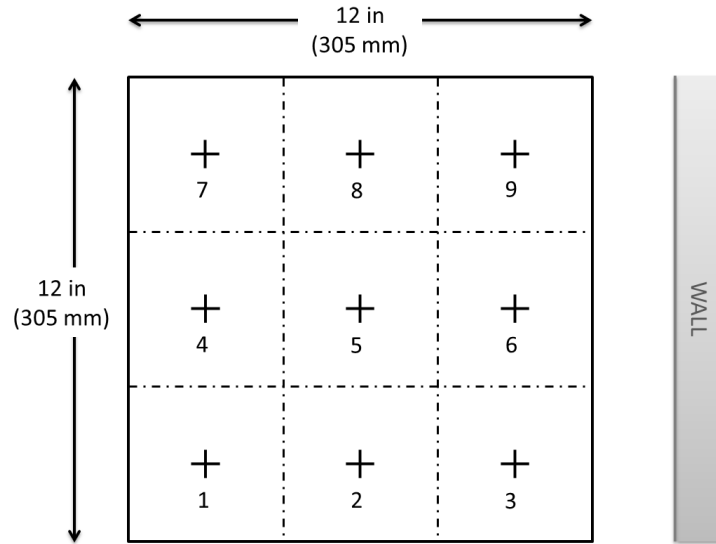


Figure 3-5: Sampling grid with nine-area points for measuring the uniformity of air velocity for small setup (ASHRAE, 2007)

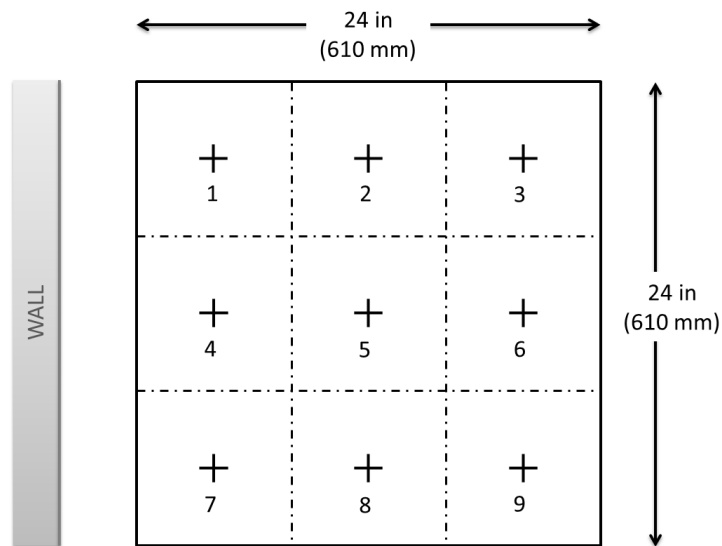
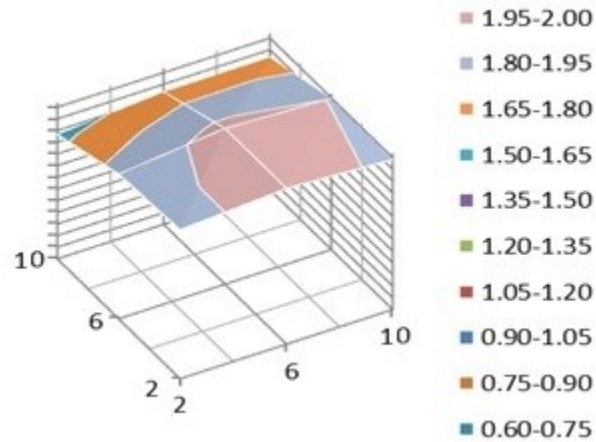


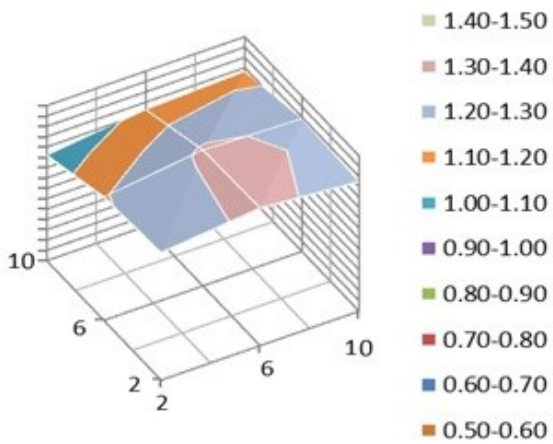
Figure 3-6: Sampling grid with nine-area points for measuring the uniformity of air velocity for big loop setup (ASHRAE, 2007)

Motor settled at 324 L/s (PANDA flowrate):

CV = 8 %



Motor settled at 203 L/s (PANDA flowrate): CV = 8 %



Motor settled at 103 L/s (PANDA flowrate): CV = 10 %

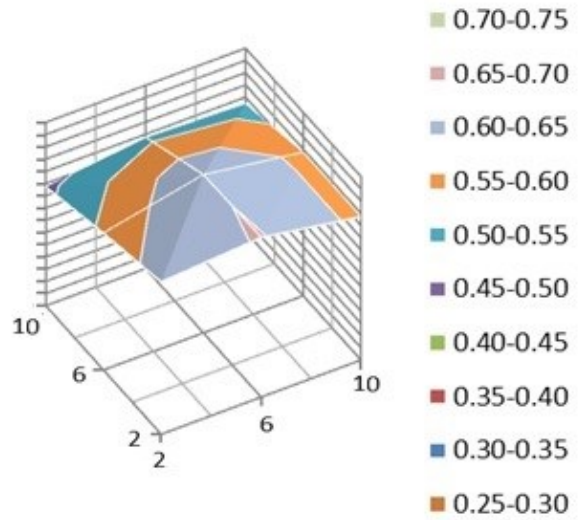
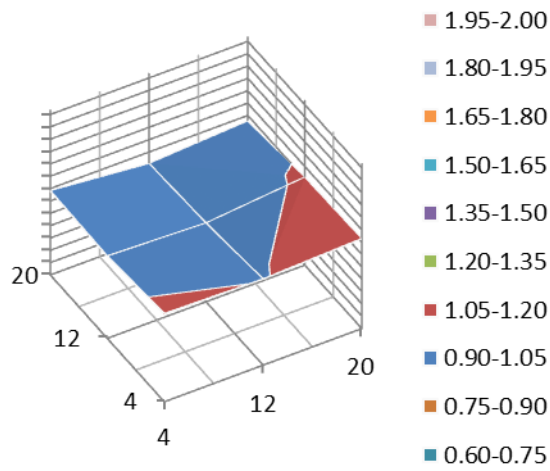
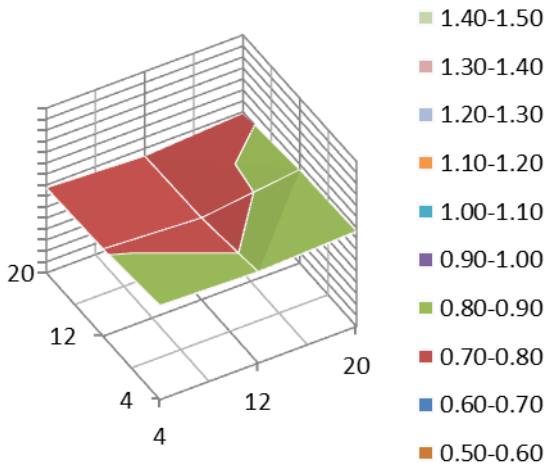


Figure 3-7: Mean of the velocity (m/s) uniformity tests at three configurations in the Small setup

Motor settled at 45 Hz
CV = 6 %



Motor settled at 35 Hz
CV = 6 %



Motor settled at 25 Hz
CV = 9 %

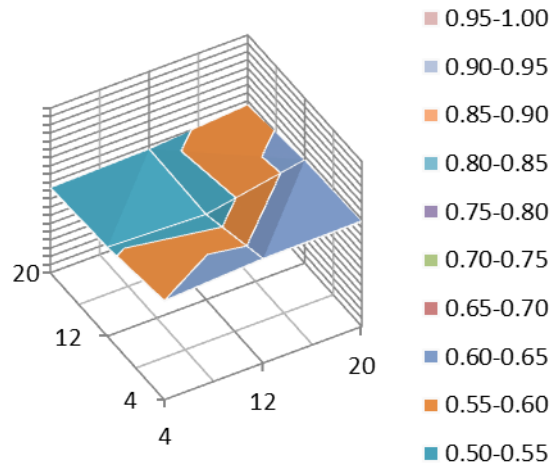


Figure 3-8: Mean of the velocity (m/s) uniformity tests at three configurations in the Big Loop setup

The coefficients of variation, shown in Figures 3-7 and 3-8, are all less than 10%, as recommended in the ASHRAE standard.

The mean velocity of nine points was then measured in three tests in order to apply a linear regression at the center of the chamber (see figure 3-9).

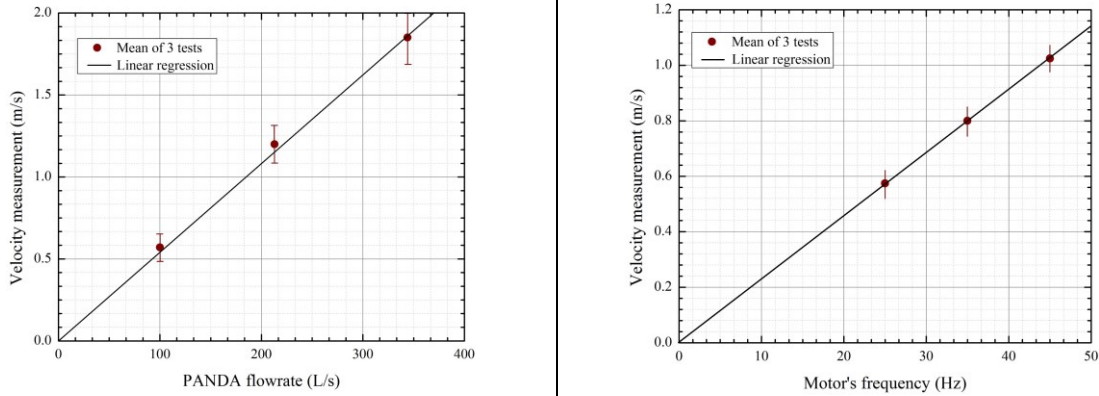


Figure 3-9: Velocity measurement at center of the upstream according to motor's characteristic – Linear regression (Left) for small setup; (Right) for big loop setup

Figure 3-9 demonstrates the linear regression of the velocity measured as a function of the engine characteristic for both small setup and big loop setup. According to these regressions, the big loop setup allows to test filters at measurement speeds ranging from 0.6 to 1 m/s. During the tests two measurement speeds are used: 0.75 m/s and 1.00 m/s, and the motor frequency to adjust them are respectively 33 Hz and 44 Hz. Also the small setup allows to test filters at measurement speeds ranging from 0.25 to 1.50 m/s. During the tests four measurement speeds will be used: 0.25 m/s, 0.50 m/s, 0.75 m/s and 1.00 m/s, and the motor flow rates to adjust them are respectively 46, 92, 139 and 186 L/s PANDA flow rate. To compare the penetration results of both setups, the measurements are conducted at 0.75 and 1 m/s.

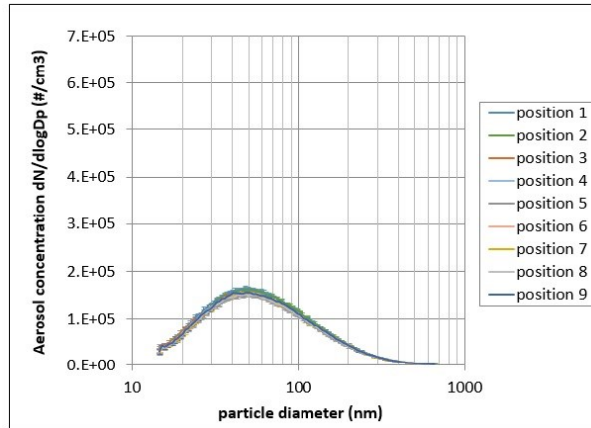
3.4.2. Stabilization test

A stabilization test has been carried out at four different constant velocities (0.25, 0.5, 0.75 and 1 m/s) for small setup and two different constant velocities (0.75 and 1m/s) for big loop setup to specify the required time length for the particles to get a steady state concentration. The required stabilization times was around 2 minutes for both setups.

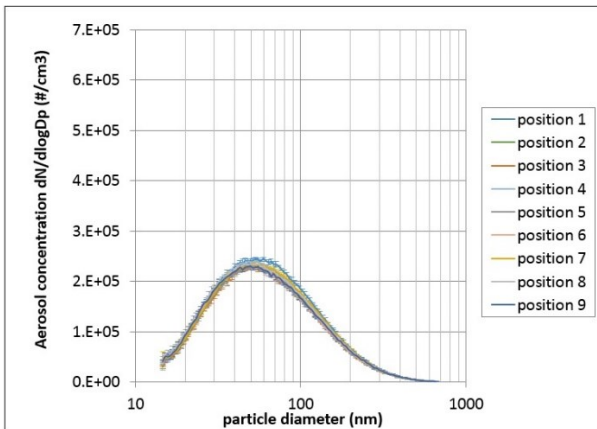
3.4.3. Aerosol homogeneity

The uniformity of the aerosol concentration across the ducts section was determined by a nine-point at the downstream section measurement for both setups. (Same sampling grid with nine-area points for measuring the uniformity of air velocity). This uniformity test has been collected at three different motor flowrate (103, 203 and 324 L/s PANDA flowrate) for small setup and two different motor frequency (33 and 44 Hz) for big loop setup. Each nine point were an average of five scan measurements. According to the standard, the coefficient of variation of the nine corresponding grid point aerosol homogeneity values shall be less than 15 % at each configuration. Figures 3-10 and 3-11 demonstrate the aerosol homogeneity for both small and big loop setups.

Motor settled at 324 L/s (PANDA flowrate)
CV = 3 %



Motor settled at 203 L/s (PANDA flowrate)
CV = 3 %



Motor settled at 103 L/s (PANDA flowrate)
CV = 2 %

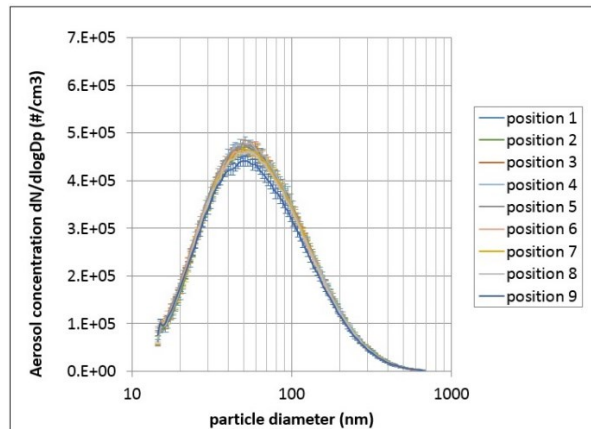
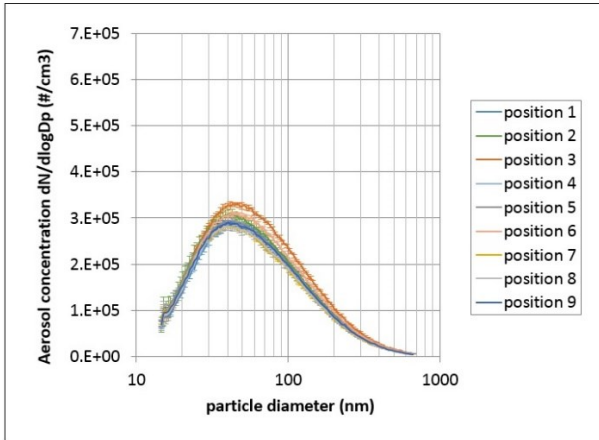


Figure 3-10: Mean of the aerosol homogeneity tests at three configurations in the Small setup

Motor settled at 44 Hz
CV = 5 %



Motor settled at 33 Hz
CV = 4 %

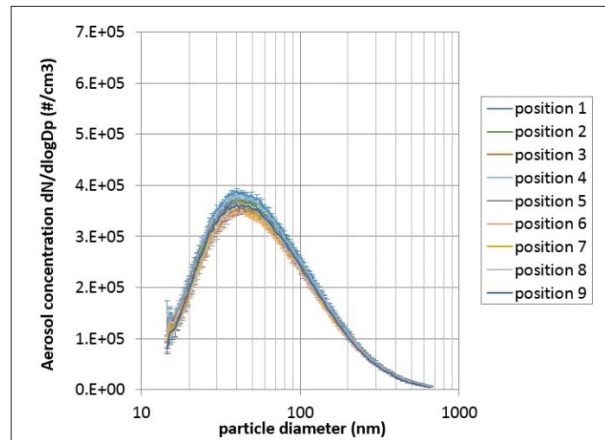


Figure 3-11: Mean of the aerosol homogeneity tests at two configurations in the Big Loop setup

The coefficients of variation, shown in Figures 3-10 and 3-11, are all less than 15%, as recommended in the ASHRAE standard.

Chapter 4: RESULTS AND DISCUSSION

4.1. Introduction

Based on the ASHRAE 52.2 standard the qualification measurements involving velocity and aerosol generation homogeneity were employed for both setups. The velocity measurements in the setups were made in order to know precisely the range of speeds accessible by the fan. Afterward the quantity, the stability and the homogeneity of the generated aerosols have been validated. Finally the penetration comparison between small setup and big loop setup is presented in this chapter. For each tested filter, the penetration measurements are compared between the small setup and the big loop setup. An overall description and analysis of the results are discussed in details. To achieve aforementioned results an experimental methodology for both small setup and big loop setup has been developed to test one type of mechanical filters rated (MERV 8) in three different depth sizes (1, 2 and 4in) to measure the initial penetration for particles smaller than 300 nm, then to validate the procedure the results from both setups are compared to each other. In addition, the effect of face velocity (0.25, 0.5, 0.75 and 1 m/s) on the initial penetration in small setup is investigated. Also, to verify the repeatability, each filter was tested three times at each related velocity. In this chapter, the outcomes of each experiment are explained and discussed in details.

4.2. Repeatability

Each filter was tested two times at four velocities: 0.25, 0.5, 0.75 and 1 m/s for small setup and at two velocities: 1 and 0.75 m/s for big loop setup in three depth sizes (1, 2 and 4in). In small setup, the maximum difference in penetration for filter 1 (N=2), filter 2 (N=2) and filter 3 (N=2) has not exceeded 7%, 10% and 10% respectively. Also in big loop setup, the maximum difference in penetration for filter 1 (N=2), filter 2 (N=2) and filter 3 (N=2) has not exceeded 10%, 9% and 9%

respectively. In conclusion the repeatability of the filters in both small and big loop setup were not exceeded 10%.

4.3. Penetration comparison between small setup and big loop setup

The penetration curves (in terms of particle size) for both small and big loop setups at 1 and 0.75 m/s in three different depth sizes (4, 2 and 1 in) are illustrated in Figures 4-1.

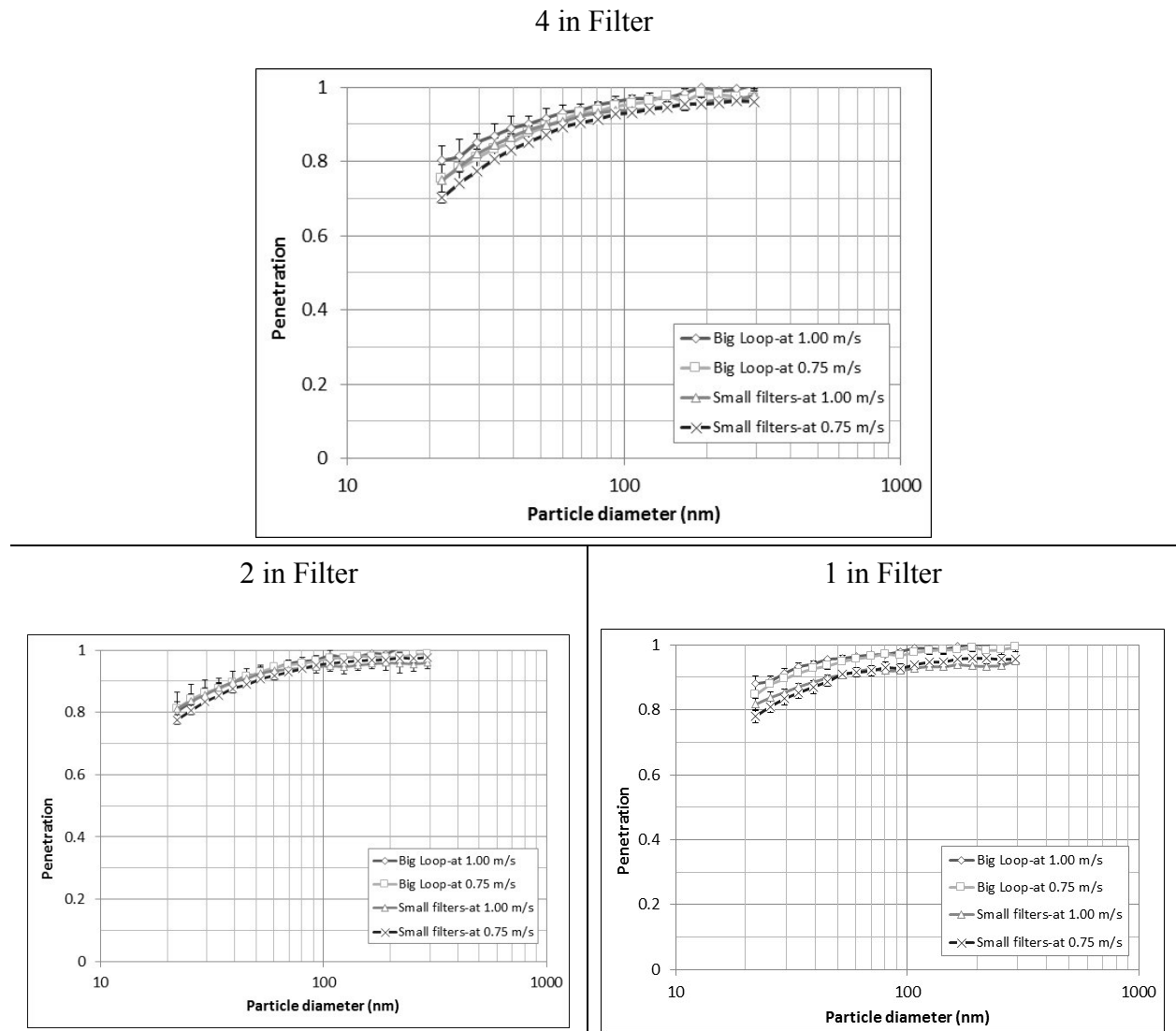


Figure 4-1: Comparison of penetration data through MERV 8 for both small setup and big loop setup at two constant velocities: 0.75 and 1 m/s. The error bars represent the standard deviations

Figures 4-1 illustrates the penetration results from both small setup and big loop setup through MERV 8 (1, 2 and 4in) at two constant velocities (1 and 0.75 m/s) when challenged with poly-disperse sodium chloride aerosols. All experimental results are presented in penetration terms with respect to the electrical mobility diameter that is classified by the long DMA. Each data point is an average of three tested filter with its standard deviations. The results demonstrate a very slight variability with small standard deviations for all tested filters in this study. As noticed in figure 4-1, the initial MPPS penetration takes place at a particle size higher than 100 nm at all face velocities for both setups in three different depth size (4, 2 and 1 in). It can also be observed that the measured penetration is less when the particle size falls below 100 nm; which is consistent with the literature (Balazy et al., 2005; Balazy et al., 2006; Huang et al., 2007; Martin Jr & Moyer, 2000).

The mean initial percentage penetrations at small setup for 4 in filter are 90.5 ± 1.5 and 88.5 ± 1.8 at 1 and 0.75 m/s respectively, for 2 in are 92.2 ± 1 and 91.7 ± 1.4 at 1 and 0.75 m/s respectively, and finally for 1 in filter are 90.7 ± 0.9 and 90.8 ± 1.3 at 1 and 0.75 m/s respectively. Similarly, at big loop setup the mean initial percentage penetrations for 4 in filter are 93.2 ± 1.4 and 91 ± 1.7 at 1 and 0.75 m/s respectively, for 2 in filter are 94.1 ± 1.4 and 93.6 ± 1.2 at 1 and 0.75 m/s respectively, and finally for 1 in filter are 96.7 ± 1 and 95.1 ± 1 at 1 and 0.75 m/s respectively.

The results from mean initial percentage penetrations for both setups in three different depth size (1, 2 and 4 in) demonstrate that aerosol penetration through the tested filters increases with increasing face velocity, and decreases as filter thickness increase. Face velocity plays a significant role in the penetration of aerosols through filter media. According to the literature the effect of face velocity on aerosol penetration is usually most important for aerosol particles $< 1 \mu\text{m}$. For mechanical filters, aerosol penetration increases with increasing face velocity due to the fact that the dominant filtration mechanisms are diffusion in this size range (Huang et al., 2013). Also

according to equation (2-1) aerosol penetration decreases with increased filter thickness. However, this conclusion is only valid for mechanical filters.

Figure 4-2 shows the complete procedure to compare the penetration results between both small setup and big loop setup. In order to compare the penetration results between both setups following steps are considered: 1) the small setup and big loop setup are designed, build and qualified; 2) the mean of the three tested filters in each three different depth size (4, 2 and 1 in) at 1 and 0.75 m/s are calculated for both setups; 3) finally the comparison between penetration results for both setups are made.

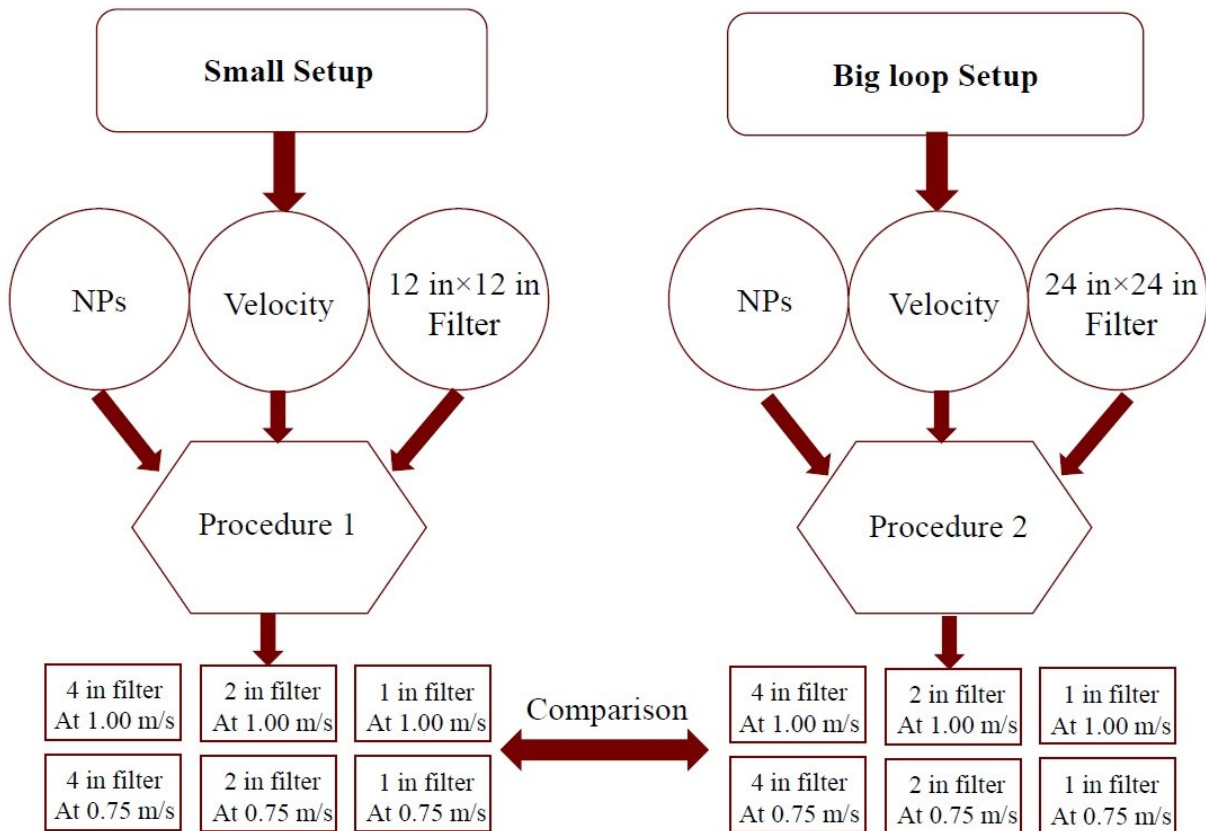


Figure 4-2: Complete procedure to compare the penetration data through MERV 8 for both small setup and big loop setup

Figure 4-3 illustrates the comparison of penetration results between both setups, The data presented in figure 4-3 show that the range of 22.1-294.3 nm gives a fairly good correlation

($R^2=0.898$) between the two setups and for the penetration range of 0.7-1.0 at 1 and 0.75 m/s. One can observe that, for this kind of filter, the big loop setup penetration measurements are slightly overestimated comparing to those obtained by the small setup in all three filter depth sizes (4, 2 and 1 in) at 0.75 and 1 m/s. This shift may be due to the differences in setups, in filters or in the procedure. However, the effect of lost in both setups is negligible and the filtration rate for the filters used in both setups is equivalent to each other.

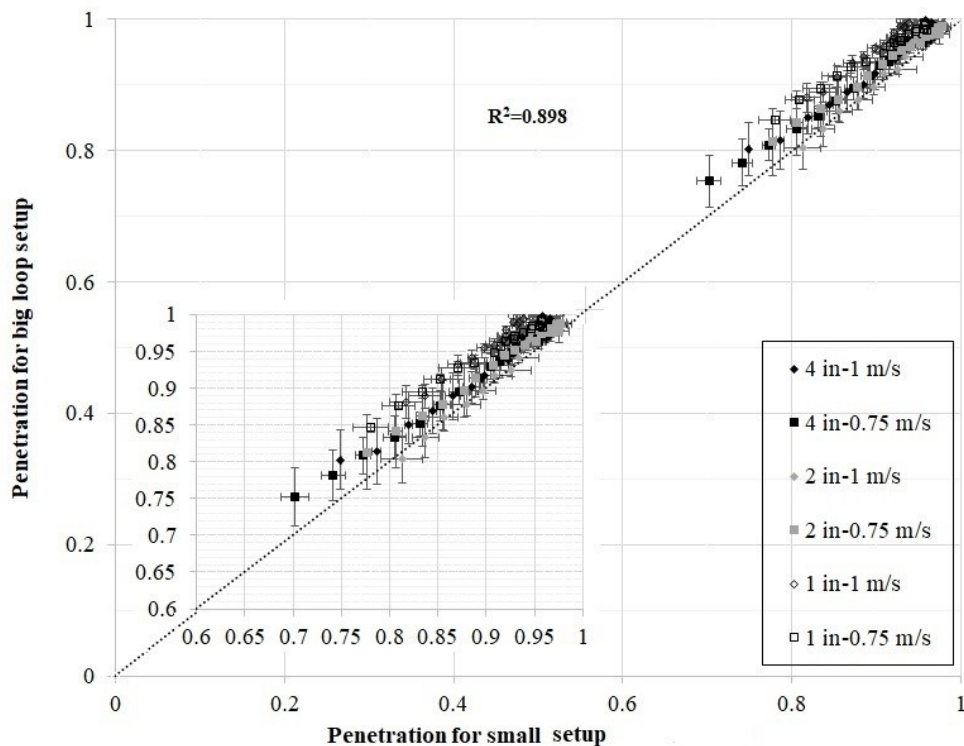


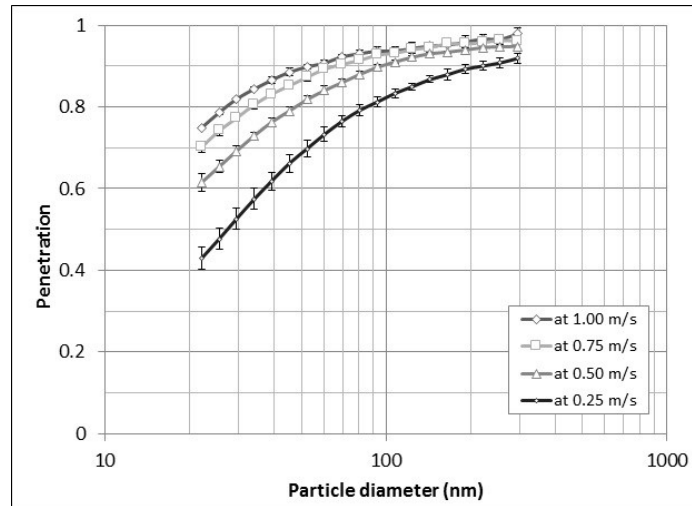
Figure 4-3: Comparison of penetration data through MERV 8 for both small setup and big loop

4.4. Effect of velocity in small setup

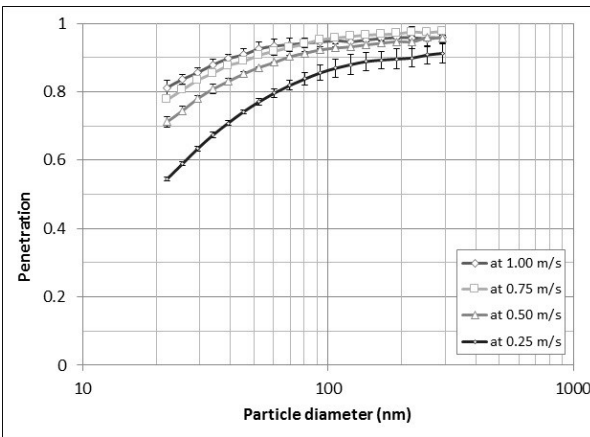
The MERV 8 (1, 2 and 4 in) filters were challenged with poly-disperse NaCl aerosols at four constant velocities: 0.25, 0.5, 0.75 and 1 m/s. Each penetration measurement (poly-dispersed; 22.1-

294.3 nm), for the four velocities was repeated 2 times (N=2), for each three filter and illustrated by the mean value and the standard deviation.

4 in Filter



2 in Filter



1 in Filter

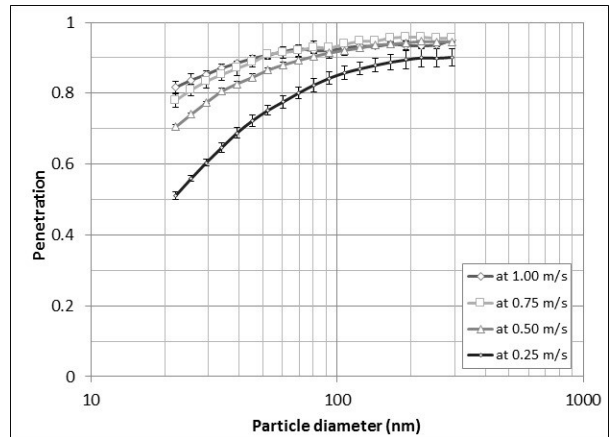


Figure 4-4: Effect of particle size and face velocity on initial particle penetration through MERV 8, in small setup. The error bars represent the standard deviations

Figures 4-4 shows the initial particle penetration values through MERV 8 at four constant velocities in three different depth size (1, 2 and 4 in) when challenged with poly-disperse sodium chloride aerosols. The results demonstrate a very high consistency with small standard deviations for all tested filter. It is clear that the measured penetration is less when the particle size falls below 100 nm. Consistent with previous studies, the initial particle penetration is significantly improved

as the face velocity increased. (Bałazy et al., 2005; Bałazy et al., 2006; Eninger et al., 2008; Huang et al., 2007). In addition, the initial MPPS penetration takes place at a particle size higher than 100 nm at all face velocities. It can also be observed that according to equation (2-1) aerosol penetration decreases with increased filter thickness, especially for 4 in filter. However, this conclusion is only valid for mechanical filters.

Chapter 5: CONCLUSIONS AND FUTURE WORK

5.1. Conclusions

The main goal of this study was to develop a methodology to evaluate the effectiveness of mechanical filters used in general ventilation systems against poly-disperse aerosols smaller than 300 nm. This methodology is then used to 1) compare the penetration results from both setups in order to validate the methodology to measure the effectiveness of these filters against NPs, 2) investigate the effect of face velocity, filter's thickness and particle size on the initial particle penetration through the one model of mechanical filter MERV 8 in three different depth size (1, 2 and 4in) in both small and big loop setup.

Challenging one type of mechanical filters (MERV 8) with poly-disperse aerosols in both small setup and big loop setup. The conclusions of this study are given as follow:

- By comparing the results from both setups it can be concluded that the range of 22.1-294.3 nm gives a fairly good correlation ($R^2=0.898$) between the two setups and for the penetration range of 0.7-1.0 at 1 and 0.75 m/s.
- The results from comparison between two setups is a firm validation for evaluating the effectiveness of mechanical filters against particles smaller than 300 nm.
- The initial particle penetration was improved with an increase in face velocity.
- The initial MPPS penetration takes place at a particle size higher than 100 nm at all face velocities for both setups in three different depth size (4, 2 and 1 in).
- The measured penetration is less when the particle size decreases below 100 nm.
- Aerosol penetration decreases with increased filter thickness. Even though the penetration curves shape should remain the same.

5.2. Recommendations and Future Work

The Recommendations for future research on filtration performance evaluations against NPs are as follows:

- The developed methodology has the capability to evaluate the filtration efficiency of series of mechanical filters (MERV 8 to HEPA) and electret filters.
- The developed methodology has the capability to measure the pressure drop of mechanical filters.
- In addition, further tests must be investigated with other filters in order to achieve better correlation between both setups.
- The effect of other parameters such as particle loading, relative humidity and particle charge state, which have an influenced on the filtration efficiency of particles smaller than 300 nm, is still need to be investigated.
- The findings of this study, is limited to the proposed experimental setups. However, further theoretical and modeling studies are highly required, to validate the experimental data, and to investigate the impact of all influencing parameters.

In conclusion, better understanding of filter media filtration characteristics, particularly in the range of nanoparticles, will help to promote the incorporation of technological developments to ensure the health of occupants.

REFERENCES

- Adam, R., Lücke, T., Tittel, R., & Fissan, H. (1992). Investigation of structure of planar inhomogeneous filter media from glass fibers. *Journal of Aerosol Science*, 23, 737-740.
- Alderman, S. L., Parsons, M. S., Hogancamp, K. U., & Waggoner, C. A. (2008). Evaluation of the effect of media velocity on filter efficiency and most penetrating particle size of nuclear grade high-efficiency particulate air filters. *Journal of Occupational and Environmental Hygiene*, 5(11), 713-720.
- Allen, M., & Raabe, O. (1982). Re-evaluation of Millikan's oil drop data for the motion of small particles in air. *Journal of Aerosol Science*, 13(6), 537-547.
- Allen, M. D., & Raabe, O. G. (1985). Slip correction measurements of spherical solid aerosol particles in an improved Millikan apparatus. *Aerosol Science and Technology*, 4(3), 269-286. Doi: 10.1080/02786828508959055
- Alonso, M., Alguacil, F., Santos, J., Jidenko, N., & Borra, J. (2007). Deposition of ultrafine aerosol particles on wire screens by simultaneous diffusion and image force. *Journal of Aerosol Science*, 38(12), 1230-1239.
- Alonso, M., Hernandez-Sierra, A., & Alguacil, F. J. (2002). Diffusion charging of aerosol nanoparticles with an excess of bipolar ions. *Journal of Physics A: Mathematical and General*, 35(30), 6271.
- Alonso, M., Kousaka, Y., Hashimoto, T., & Hashimoto, N. (1997). Penetration of nanometer-sized aerosol particles through wire screen and laminar flow tube. *Aerosol Science and Technology*, 27(4), 471-480. Doi: 10.1080/02786829708965487
- Andersen, S. K., Johannessen, T., Mosleh, M., Wedel, S., Tranto, J., & Livbjerg, H. (2002). The formation of porous membranes by filtration of aerosol nanoparticles. *Journal of Nanoparticle Research*, 4(5), 405-416.
- ASHRAE, A. S. (2007). Standard 52.2-2007. Method of testing general ventilation air cleaning devices for removal efficiency by particle size, in. *American Society of Heating, Refrigerating, and Air Conditioning Engineers, Inc. Atlanta*,
- Bahloul, A., Mahdavi, A., Haghghat, F., & Ostiguy, C. (2014). Evaluation of N95 filtering facepiece respirator efficiency with cyclic and constant flows. *Journal of Occupational and Environmental Hygiene*, 11(8), 499-508. doi:10.1080/15459624.2013.877590
- Bałazy, A., & Podgórski, A. (2007). Deposition efficiency of fractal-like aggregates in fibrous filters calculated using Brownian dynamics method. *Journal of Colloid and Interface Science*, 311(2), 323-337.

- Bałaży, A., Toivola, M., Adhikari, A., Sivasubramani, S. K., Reponen, T., & Grinshpun, S. A. (2006). Do N95 respirators provide 95% protection level against airborne viruses, and how adequate are surgical masks? *American Journal of Infection Control*, 34(2), 51-57.
- Bałaży, A., Toivola, M., Reponen, T., Podgórski, A., Zimmer, A., & Grinshpun, S. A. (2005). Manikin-based performance evaluation of N95 filtering-facepiece respirators challenged with nanoparticles. *Annals of Occupational Hygiene*, 50(3), 259-269.
- Balazy, A., Podgorski, A., & Gradon, L. (2004). Filtration of nano-sized aerosol particles in fibrous filters. I-experimental results. *Journal of Aerosol Science*, 35(2), 967-968.
- Bao, L., Otani, Y., Namiki, N., Mori, J., & Emi, H. (1998). Prediction of HEPA filter collection efficiency with a bimodal fiber size distribution. *Kagaku Kogaku Ronbunshu*, 24(5), 766-771.
- Bergman, W., Taylor, R., & Miller, H. (1978). 15th DOE nuclear air cleaning conference. Paper presented at the *CONF-780819, Boston*,
- Biskos, G., Russell, L., Buseck, P., & Martin, S. T. (2006). Nano-size effect on the hygroscopic growth factor of aerosol particles. *Geophysical Research Letters*, 33(7)
- Borm, P. J., & Kreyling, W. (2004). Toxicological hazards of inhaled nanoparticles—potential implications for drug delivery. *Journal of Nanoscience and Nanotechnology*, 4(5), 521-531.
- Boskovic, L., Altman, I. S., Agranovski, I. E., Braddock, R. D., Myojo, T., & Choi, M. (2005). Influence of particle shape on filtration processes. *Aerosol Science and Technology*, 39(12), 1184-1190.
- Boskovic, L., Agranovski, I. E., & Braddock, R. D. (2007). Filtration of nano-sized particles with different shape on oil coated fibers. *Journal of Aerosol Science*, 38, 1220-1229.
- Boskovic, L., Agranovski, I. E., Altman, I. S., & Braddock, R. D. (2008). *Filter efficiency as a function of nanoparticle velocity and shape*
doi:<http://dx.doi.org/10.1016/j.jaerosci.2008.03.003>
- Bourrous, S. (2014). *Étude Du Colmatage Des Filtres THE Plans Et À Petits Plis Par Des Agrégats De Nanoparticules Simulant Un Aérosol De Combustion*,
- Bourrous, S., Bouilloux, L., Ouf, F. -, Lemaitre, P., Nerisson, P., Thomas, D., & Appert-Collin, J. C. (2016). *Measurement and modeling of pressure drop of HEPA filters clogged with ultrafine particles* doi:<http://dx.doi.org/10.1016/j.powtec.2015.11.020>
- Brochot, C., Abdolghader, P., Haghigat, F., & Bahloul, A. (2018). Filtration of nanoparticles applied in general ventilation. *Science and Technology for the Built Environment*, (just-accepted), 1-27.

- Brock, S., & Tarleton, E. (1998). The use of fractal dimensions in filtration.
- Brown, R. C. (1993). *Air filtration: An integrated approach to the theory and applications of fibrous filters* Pergamon.
- Callé, S. (2000). *Etude Des Performances Des Media Filtrants Utilisés En Dépoussiérage Industriell*,
- Chang, D., Chen, S., Fox, A. R., Viner, A. S., & Pui, D. Y. (2015). Penetration of sub-50 nm nanoparticles through electret HVAC filters used in residence. *Aerosol Science and Technology*, 49(10), 966-976.
- Chang, D., Chen, S., & Pui, D. Y. (2016). Capture of sub-500 nm particles using residential electret HVAC filter media-experiments and modeling. *Aerosol and Air Quality Research*, 16(12), 3349-3357.
- Chen, C. Y. (1955). Filtration of aerosols by fibrous media. *Chemical Reviews*, 55(3), 595-623.
- Chen, F. (1975). *The Permeability of Compressed Fiber Mats and the Effects of Surface Area Reduction and Fiber Geometry*,
- Cheng, Y., & Yeh, H. (1980). Theory of a screen-type diffusion battery. *Journal of Aerosol Science*, 11(3), 313-320.
- Davies, C. N. (1973). Air filtration.
- Davies, C. (1953). The separation of airborne dust and particles. *Proceedings of the Institution of Mechanical Engineers, Part B: Management and Engineering Manufacture*, 1(1-12), 185-213.
- De Freitas, N. L., Gonçalves, J. A., Innocentini, M. D., & Coury, J. R. (2006). Development of a double-layered ceramic filter for aerosol filtration at high-temperatures: The filter collection efficiency. *Journal of Hazardous Materials*, 136(3), 747-756.
- Dhaniyala, S., & Liu, B. Y. (2001a). Experimental investigation of local efficiency variation in fibrous filters. *Aerosol Science & Technology*, 34(2), 161-169.
- Dhaniyala, S., & Liu, B. Y. (2001b). Theoretical modeling of filtration by non-uniform fibrous filters. *Aerosol Science & Technology*, 34(2), 170-178.
- Endo, Y., Chen, D., & Pui, D. Y. (2002). Theoretical consideration of permeation resistance of fluid through a particle packed layer. *Powder Technology*, 124(1), 119-126.
- Eninger, R. M., Honda, T., Adhikari, A., Heinonen-Tanski, H., Reponen, T., & Grinshpun, S. A. (2008). Filter performance of N99 and N95 facepiece respirators against viruses and ultrafine particles. *Annals of Occupational Hygiene*, 52(5), 385-396.

- Fowler, J., & Hertel, K. (1940). Flow of a gas through porous media. *Journal of Applied Physics*, 11(7), 496-502.
- Fuchs, N. (1963). On the stationary charge distribution on aerosol particles in a bipolar ionic atmosphere. *Pure and Applied Geophysics*, 56(1), 185-193.
- Fuchs, N., & Stechkina, I. (1963). A note on the theory of fibrous aerosol filters. *The Annals of Occupational Hygiene*, 6(1), 27-30.
- Givehchi, R. (2016). Filtration of NaCl and WO_x nanoparticles using wire screens and nano fibrous filters.
- Givehchi, R., Li, Q., & Tan, Z. (2015). *The effect of electrostatic forces on filtration efficiency of granular filters* doi:<https://doi.org/10.1016/j.powtec.2015.01.074>
- Gupta, A., Novick, V. J., Biswas, P., & Monson, P. R. (1993). Effect of humidity and particle hygroscopicity on the mass loading capacity of high efficiency particulate air (HEPA) filters. *Aerosol Science and Technology*, 19(1), 94-107. Doi: 10.1080/02786829308959624
- Hanley, J., Ensor, D., Smith, D., & Sparks, L. (1994). Fractional aerosol filtration efficiency of in- duct ventilation air cleaners. *Indoor Air*, 4(3), 169-178.
- Happel, J. (1959). Viscous flow relative to arrays of cylinders. *AIChE Journal*, 5(2), 174-177. doi:10.1002/aic.690050211
- Hecker, R., & Hofacre, K. (2008). Development of performance data for common building air cleaning devices (final report no. EPA/600/R-08/013). *US Environmental Protection Agency, Office of Research and Development/National Homeland Security Research Center Research Triangle Park, NC*,
- Heidenreich, E., Tittel, R., Neuber, A., & Adam, R. (1991). Measuring the inhomogeneities of high efficient glass fiber filter media. *Journal of Aerosol Science*, 22, S785-S788.
- Hemmer, G., Hoff, D., & Kasper, G. (2003). Thermo-analysis of fly ash and other particulate materials for predicting stable filtration of hot gases. *Advanced Powder Technology*, 14(6), 631-655.
- Henry, F. s., & Ariman, T. (1983). An evaluation of the Kuwabara model. *Particulate Science and Technology*, 1(1), 1-20.
- Hinds, W. C. (1999). *Aerosol technology: Properties, behavior, and measurement of airborne particles*. New York: Wiley. Retrieved from <http://www.loc.gov/catdir/toc/onix02/98023683.html>

- Hinds, W. C., & Kadrichu, N. P. (1997). The effect of dust loading on penetration and resistance of glass fiber filters. *Aerosol Science and Technology*, 27(2), 162-173. Doi: 10.1080/02786829708965464
- Hogan, C. J., Li, L., Chen, D., & Biswas, P. (2009). Estimating aerosol particle charging parameters using a Bayesian inversion technique. *Journal of Aerosol Science*, 40(4), 295-306.
- Hoppel, W. A., & Frick, G. M. (1986). Ion—aerosol attachment coefficients and the steady-state charge distribution on aerosols in a bipolar ion environment. *Aerosol Science and Technology*, 5(1), 1-21.
- Hu, D., Qiao, L., Chen, J., Ye, X., Yang, X., Cheng, T., & Fang, W. (2010). Hygroscopicity of inorganic aerosols: Size and relative humidity effects on the growth factor. *Aerosol Air Qual. Res.*, 10, 255-264.
- Huang, S., Chen, C., Chang, C., Lai, C., & Chen, C. (2007). Penetration of 4.5 nm to 10 μ m aerosol particles through fibrous filters. *Journal of Aerosol Science*, 38(7), 719-727.
- Huang, S., Chen, C., Kuo, Y., Lai, C., McKay, R., & Chen, C. (2013). Factors affecting filter penetration and quality factor of particulate respirators. *Aerosol and Air Quality Research*, 13(1), 162-171.
- Hung, C., & Leung, W. W. (2011). Filtration of nano-aerosol using nanofiber filter under low Peclet number and transitional flow regime. *Separation and Purification Technology*, 79(1), 34-42.
- Ichitsubo, H., Hashimoto, T., Alonso, M., & Kousaka, Y. (1996). Penetration of ultrafine particles and ion clusters through wire screens. *Aerosol Science and Technology*, 24(3), 119-127. Doi: 10.1080/02786829608965357
- Ikezaki, K., Iritani, K., Nakamura, T., & Hori, T. (1995). Charge stability of TPX film electrets. *Journal of Electrostatics*, 35(1), 41-46.
- Ingmanson, W., & Andrews, B. (1963). High velocity water flow through fiber mats. *Tappi*, 46(3), 150-155.
- Jackson, G. W., & James, D. F. (1986). The permeability of fibrous porous media. *The Canadian Journal of Chemical Engineering*, 64(3), 364-374.
- Jeon, K., & Jung, Y. (2004). A simulation study on the compression behavior of dust cakes. *Powder Technology*, 141(1), 1-11.
- Joubert, A. (2009). Performances des filtres plissés à très haute efficacité en fonction de l'humidité relative de l'air. *ISR.N. Novembre*,

- Joubert, A., Laborde, J., Bouilloux, L., Calle-Chazelet, S., & Thomas, D. (2010). Influence of humidity on clogging of flat and pleated HEPA filters. *Aerosol Science and Technology*, 44(12), 1065-1076.
- Joubert, A., Laborde, J. C., Bouilloux, L., Chazelet, S., & Thomas, D. (2011). *Modelling the pressure drop across HEPA filters during cake filtration in the presence of humidity* doi:<http://dx.doi.org/10.1016/j.cej.2010.11.033>
- Juda, J., & Chrosciel, S. (1970). Ein theoretisches modell der druckverlusthöhung beim filtrationsvorgang. *Staub Reinhaltung Der Luft*, 5, 196-198.
- Kanaoka, C., & Hiragi, S. (1990). Pressure drop of air filter with dust load. *Journal of Aerosol Science*, 21(1), 127133-131137.
- Kanaoka, C., Emi, H., Otani, Y., & Iiyama, T. (1987). Effect of charging state of particles on electret filtration. *Aerosol Science and Technology*, 7(1), 1-13. Doi: 10.1080/02786828708959142
- Karjalainen, P., Saari, S., Kuuluvainen, H., Kalliohaka, T., Taipale, A., & Rönkkö, T. (2017). Performance of ventilation filtration technologies on characteristic traffic related aerosol down to nanocluster size. *Aerosol Science and Technology*, 51(12), 1398-1408.
- Kasper, G., Schollmeier, S., & Meyer, J. (2010). Structure and density of deposits formed on filter fibers by inertial particle deposition and bounce. *Journal of Aerosol Science*, 41(12), 1167-1182.
- Kasper, G., Preining, O., & Matteson, M. (1978). Penetration of a multistage diffusion battery at various temperatures. *Journal of Aerosol Science*, 9(4), 331-338.
- Kim, C. S., Bao, L., Okuyama, K., Shimada, M., & Niinuma, H. (2006). Filtration efficiency of a fibrous filter for nanoparticles. *Journal of Nanoparticle Research*, 8(2), 215-221.
- Kim, S. C., Harrington, M. S., & Pui, D. Y. (2007). Experimental study of nanoparticles penetration through commercial filter media. *Journal of Nanoparticle Research*, 9(1), 117-125.
- Kim, S. C., Wang, J., Shin, W. G., Scheckman, J. H., & Pui, D. Y. H. (2009). Structural properties and filter loading characteristics of soot agglomerates. *Aerosol Science and Technology*, 43(10), 1033-1041. Doi: 10.1080/02786820903131081
- Kirsch, A., & Fuchs, N. (1968). Studies on fibrous aerosol filters—III diffusional deposition of aerosols in fibrous filters. *Annals of Occupational Hygiene*, 11(4), 299-304.
- Kirsch, A., & Lahtin, U. (1975). Gas flow in high-porous layers of high-dispersed particles. *Journal of Colloid and Interface Science*, 52(2), 270-276.

- Kirsch, A., & Stechkina, I. (1973). Pressure drop and diffusional deposition of aerosol in polydisperse model filter. *Journal of Colloid and Interface Science*, 43(1), 10-16.
- Kirsch, A., Stechkina, I., & Fuchs, N. (1974). Gas flow in aerosol filters made of polydisperse ultrafine fibers. *Journal of Aerosol Science*, 5(1), 39-45.
- Kirsch, A., & Zhulanov, U. V. (1978a). Measurement of aerosol penetration through high efficiency filters. *Journal of Aerosol Science*, 9(4), 291-298.
- Kirsch, A., & Zhulanov, U. V. (1978b). Measurement of aerosol penetration through high efficiency filters. *Journal of Aerosol Science*, 9(4), 291-298.
- KIRSCH, V. (1998). Method for the calculation of an increase in the pressure drop in an aerosol filter on clogging with solid particles. *Colloid Journal of the Russian Academy of Sciences: Kolloidnyi Zhurnal*, 60, 439-443.
- Kirsh, A., & Stechkina, I. (1978). The theory of aerosol filtration with fibrous filter: Fundamentals of aerosol science. NY: Wiley, 165.
- Kousaka, Y., Okuyama, K., Shimada, M., & Takii, Y. (1990). Development of a method for testing very high-efficiency membrane filters for ultrafine aerosol particles. *Journal of Chemical Engineering of Japan*, 23(5), 568-574.
- Kraemer, H. F., & Johnstone, H. (1955). Collection of aerosol particles in presence of electrostatic fields. *Industrial & Engineering Chemistry*, 47(12), 2426-2434.
- Kreyling, W. G., Semmler, M., & Möller, W. (2004). Dosimetry and toxicology of ultrafine particles. *Journal of Aerosol Medicine*, 17(2), 140-152.
- Kuwabara, S. (1959). The forces experienced by randomly distributed parallel circular cylinders or spheres in a viscous flow at small Reynolds numbers. *Journal of the Physical Society of Japan*, 14(4), 527-532.
- Langmuir, I. (1942). Report on smokes and filters, OSRD 865. Washington, DC: Office of Scientific Research and Development, Office of Technical Services,
- Langmuir, I., Rodebush, W., & Lamer, V. (1942). Filtration of aerosols and development of filter materials. OSRD-865, Office of Scientific Research and Development, Washington, DC,
- Lathrache, R., & Fissan, H. (1987). Enhancement of particle deposition in filters due to electrostatic effects. *Filtration & Separation*, 24(6), 418-422.
- Lee, K., & Liu, B. (1982). Theoretical study of aerosol filtration by fibrous filters. *Aerosol Science and Technology*, 1(2), 147-161.

- Lee, K. W., & Gieseke, J. A. (1979). Collection of aerosol particles by packed beds. *Environmental Science & Technology*, 13(4), 466-470.
- Letourneau, P., Mulcey, P., & Vendel, J. (1991). *Aerosol penetration inside HEPA filtration media*. (). United States:
- Letourneau, P., Vendel, J., & Renaudin, V. (1993). *Effects of the particle penetration inside the filter medium of the HEPA filter pressure drop*. (). United States:
- Liu, B. Y., & Rubow, K. L. (1990). Efficiency, pressure drop and figure of merit of high efficiency fibrous and membrane filter media. Paper presented at the *Proceedings of the Fifth World Filtration Congress, Nice*,
- Liu, J., Swanson, J. J., Kittelson, D. B., Pui, D. Y. H., & Wang, J. (2013). *Microstructural and loading characteristics of diesel aggregate cakes*
doi:<http://dx.doi.org/10.1016/j.powtec.2013.03.028>
- Loeb, L. B. (1961). *The kinetic theory of gases, being a text and reference book whose purpose is to combine the classical deductions with recent experimental advances in a convenient form for student and investigator* (3rd ed.). New York: Dover Publications.
- Łowkis, B., & Motyl, E. (2001). Electret properties of polypropylene fabrics. *Journal of Electrostatics*, 51, 232-238.
- Lundgren, D. A., & Whitby, K. (1965). Effect of particle electrostatic charge on filtration by fibrous filters. *Industrial & Engineering Chemistry Process Design and Development*, 4(4), 345-349.
- Mahdavi, A., Haghghat, F., Bahloul, A., Brochot, C., & Ostiguy, C. (2015). Particle loading time and humidity effects on the efficiency of an N95 filtering facepiece respirator model under constant and inhalation cyclic flows. *The Annals of Occupational Hygiene*, 59(5), 629-640. doi:<https://doi.org/10.1093/annhyg/mev005>
- Marlow, W., & Brock, J. (1975). Calculations of bipolar charging of aerosols. *Journal of Colloid and Interface Science*, 51(1), 23-31.
- Martin Jr, S. B., & Moyer, E. S. (2000). Electrostatic respirator filter media: Filter efficiency and most penetrating particle size effects. *Applied Occupational and Environmental Hygiene*, 15(8), 609-617.
- Matteson, M. J. (Ed.). (1987). *Filtration: Principles and practices* (2nd ed.). New York: Marcel Dekker Inc.
- Mauret, E., & Renaud, M. (1997). Transport phenomena in multi-particle systems—II. Proposed new model based on flow around submerged objects for sphere and fiber beds-transition

- between the capillary and particulate representations. *Chemical Engineering Science*, 52(11), 1819-1834.
- Miecret, G., & Gustavsson, J. (1989). Mathematic expression of HEPA filters efficiency experimental verification practical alliance to new efficiency test methods. *Contaminexpert, Versailles, France*,
- Miguel, A. (2003). Effect of air humidity on the evolution of permeability and performance of a fibrous filter during loading with hygroscopic and non-hygroscopic particles. *Journal of Aerosol Science*, 34(6), 783-799.
- Mills, N. L., Donaldson, K., Hadoke, P. W., Boon, N. A., MacNee, W., Cassee, F. R., Newby, D. E. (2009). Adverse cardiovascular effects of air pollution. *Nature Clinical Practice. Cardiovascular Medicine*, 6(1), 36-44. Doi: 10.1038/ncpcardio1399
- Molter, W., & Fissan, H. (1997). Modelling of inhomogeneous fibrous filter media-discussion and application of the representative element size to calculate the filtration performance numerically. *Gefahrstoffe Reinhaltung Der Luft*, 57(5), 201-205.
- Montgomery, J. F., Green, S. I., & Rogak, S. N. (2015). Impact of relative humidity on HVAC filters loaded with hygroscopic and non-hygroscopic particles. *Aerosol Science and Technology*, 49(5), 322-331.
- Mostofi, R., Wang, B., Haghghat, F., Bahloul, A., & Lara, J. (2010). *Performance of mechanical filters and respirators for capturing nanoparticles-limitations and future direction* doi:10.2486/indhealth.48.296
- Mouret, G., Chazelet, S., Thomas, D., & Bemer, D. (2011). Discussion about the thermal rebound of nanoparticles. *Separation and Purification Technology*, 78(2), 125-131.
- Natanson, G. (1957). Diffusive deposition of aerosols on a cylinder in a flow in the case of small capture coefficients. *Doklady Akademii Nauk SSSR*, 112(1), 100-103.
- Novick, V. J., Higgins, P. J., Dierkschiede, B., Abrahamson, C., Richardson, W. B., Monson, P. R., & Ellison, P. G. (1991). *Efficiency and mass loading characteristics of a typical HEPA filter media material*. (). United States:
- Oberdörster, G. (2010). Safety assessment for nanotechnology and nanomedicine: Concepts of nanotoxicology. *Journal of Internal Medicine*, 267(1), 89-105.
- Otani, Y., Emi, H., & Mori, J. (1993). Initial collection efficiency of electret filter and its durability for solid and liquid particles [translated]. *KONA Powder and Particle Journal*, 11, 207-214.

- Payatakes, A., & Gradoń, L. (1980). Dendritic deposition of aerosols by convective Brownian diffusion for small, intermediate and high particle Knudsen numbers. *AIChE Journal*, 26(3), 443-454.
- Payatakes, A., & Okuyama, K. (1982). Effects of aerosol particle deposition on the dynamic behavior of uniform or multilayer fibrous filters. *Journal of Colloid and Interface Science*, 88(1), 55-78.
- Payet, S., Boulaud, D., Madelaine, G., & Renoux, A. (1992). Penetration and pressure drop of a HEPA filter during loading with submicron liquid particles. *Journal of Aerosol Science*, 23(7), 723-735.
- Penicot Baugé, P. (1998). *Étude De La Performance De Filtres À Fibres Lors De La Filtration D'Aérosols Liquides Ou Solides Submicroniques*,
- Pich, J. (1965). The filtration theory of highly dispersed aerosols. *Staub Reinhalt*, 5, 16-23.
- Pich, J. (1966). The effectiveness of the barrier effect in fiber filters at small Knudsen numbers. *Staub Reinhalt*, 26, 1-4.
- Podgórski, A., Bałazy, A., & Gradoń, L. (2006). Application of nanofibers to improve the filtration efficiency of the most penetrating aerosol particles in fibrous filters. *Chemical Engineering Science*, 61(20), 6804-6815.
- Przekop, R., & Gradoń, L. (2008). Deposition and filtration of nanoparticles in the composites of nano- and micro-sized fibers. *Aerosol Science and Technology*, 42(6), 483-493. Doi: 10.1080/02786820802187077
- Punčochář, M., & Drahoš, J. (2000). *Limits of applicability of capillary model for pressure drop correlation* doi:[http://dx.doi.org/10.1016/S0009-2509\(00\)00025-7](http://dx.doi.org/10.1016/S0009-2509(00)00025-7)
- Rao, N., & Faghri, M. (1988). Computer modeling of aerosol filtration by fibrous filters. *Aerosol Science and Technology*, 8(2), 133-156.
- Sakano, T., Otani, Y., Namiki, N., & Emi, H. (2000). Particle collection of medium performance air filters consisting of binary fibers under dust loaded conditions. *Separation and Purification Technology*, 19(1), 145-152.
- Schmidt, E., & Löffler, F. (1991). The analysis of dust cake structures. *Particle & Particle Systems Characterization*, 8(1- 4), 105-109.
- Shapiro, M., Gutfinger, C., & Laufer, G. (1988). Electrostatic mechanisms of aerosol collection by granular filters: A review. *Journal of Aerosol Science*, 19(6), 651-677.

- Shi, B., Ekberg, L. E., & Langer, S. (2013). Intermediate air filters for general ventilation applications: An experimental evaluation of various filtration efficiency expressions. *Aerosol Science and Technology*, 47(5), 488-498.
- Shin, W., Mulholland, G., Kim, S., & Pui, D. (2008). Experimental study of filtration efficiency of nanoparticles below 20nm at elevated temperatures. *Journal of Aerosol Science*, 39(6), 488-499.
- Spielman, L., & Goren, S. L. (1968). Model for predicting pressure drop and filtration efficiency in fibrous media. *Environmental Science & Technology*, 2(4), 279-287.
- Stechkina, I., & Fuchs, N. (1966). Studies on fibrous aerosol filters-I. calculation of diffusional deposition of aerosols in fibrous filters. *Annals of Occupational Hygiene*, 9(2), 59-64.
- Stechkina, I., Kirsch, A., & Fuchs, N. (1969). Studies on fibrous aerosol filters-IV calculation of aerosol deposition in model filters in the range of maximum penetration. *Annals of Occupational Hygiene*, 12(1), 1-8.
- Steffens, J., & Coury, J. (2007). Collection efficiency of fiber filters operating on the removal of nano-sized aerosol particles: I—Homogeneous fibers. *Separation and Purification Technology*, 58(1), 99-105.
- Stenhouse, J. (1974). The influence of electrostatic forces in fibrous filtration. *Filtration and Separation*, 11, 25-26.
- Stephens, B., & Siegel, J. (2013). Ultrafine particle removal by residential heating, ventilating, and air- conditioning filters. *Indoor Air*, 23(6), 488-497.
- Tan, Z. (2014). *Air pollution and greenhouse gases: From basic concepts to engineering applications for air emission control* Springer.
- Tennal, K., Mazumder, M., Siag, A., & Reddy, R. (1991). Effect of loading with AIM oil aerosol on the collection efficiency of an electret filter. *Particulate Science and Technology*, 9(1-2), 19-29.
- Thomas, D., Penicot, P., Contal, P., Leclerc, D., & Vendel, J. (2001). Clogging of fibrous filters by solid aerosol particles experimental and modelling study. *Chemical Engineering Science*, 56(11), 3549-3561.
- Thomas, D., Mouret, G., Cadavid-Rodriguez, M., Chazelet, S., & Bemer, D. (2013). An improved model for the penetration of charged and neutral aerosols in the 4 to 80nm range through stainless steel and dielectric meshes. *Journal of Aerosol Science*, 57, 32-44.
- Thomas, D., Ouf, F. X., Gensdarmes, F., Bourrous, S., & Bouilloux, L. (2014). *Pressure drop model for nanostructured deposits* doi:<http://dx.doi.org/10.1016/j.seppur.2014.09.032>

- Wang, C. (2001). Electrostatic forces in fibrous filters—a review. *Powder Technology*, 118(1), 166-170.
- Wang, J., Chen, D., & Pui, D. (2007). Modeling of filtration efficiency of nanoparticles in standard filter media. *Journal of Nanoparticle Research*, 9(1), 109-115.
- Wang, J., Kim, S. C., & Pui, D. Y. (2008). Investigation of the figure of merit for filters with a single nanofiber layer on a substrate. *Journal of Aerosol Science*, 39(4), 323-334.
- Willeke, K. (1976). Temperature dependence of particle slip in a gaseous medium. *Journal of Aerosol Science*, 7(5), 381-387.
- Wise, M. E., Martin, S. T., Russell, L. M., & Buseck, P. R. (2008). Water uptake by NaCl particles prior to deliquescence and the phase rule. *Aerosol Science and Technology*, 42(4), 281-294.
- Yang, S., & Lee, G. W. (2005). Filtration characteristics of a fibrous filter pretreated with anionic surfactants for monodisperse solid aerosols. *Journal of Aerosol Science*, 36(4), 419-437.
- Yoshioka, N., Emi, H., Hattori, M., & Tamori, I. (1968). Effect of electrostatic force in the filtration efficiency of aerosols. *Kagaku Kogaku*, 32, 815-820.
- Yu, A., Bridgwater, J., & Burbidge, A. (1997). On the modelling of the packing of fine particles. *Powder Technology*, 92(3), 185-194.
- Yu, A., Feng, C., Zou, R., & Yang, R. (2003). On the relationship between porosity and interparticle forces. *Powder Technology*, 130(1), 70-76.
- Yun, K. M., Hogan, C. J., Matsubayashi, Y., Kawabe, M., Iskandar, F., & Okuyama, K. (2007). Nanoparticle filtration by electrospun polymer fibers. *Chemical Engineering Science*, 62(17), 4751-4759.
- Zhu, M., Han, J., Wang, F., Shao, W., Xiong, R., Zhang, Q., Zhang, F. (2017). Electrospun nanofibers membranes for effective air filtration. *Macromolecular Materials and Engineering*, 302(1)